Chemical Geology 312–313 (2012) 93–117

Contents lists available at SciVerse ScienceDirect

Chemical Geology

journal homepage: www.elsevier.com/locate/chemgeo

Research paper

Behavior of fluid-mobile elements in serpentines from abyssal to subduction environments: Examples from Cuba and Dominican Republic

Fabien Deschamps [a,b,*], Marguerite Godard [b], Stéphane Guillot [a], Catherine Chauvel [a], Muriel Andreani [c], Kéiko Hattori [d], Bernd Wunder [e], Lydéric France [f]

[a] ISTerre, CNRS, Université Grenoble I, 1381 rue de la Piscine, 38400 Grenoble Cedex 09, France
[b] Géosciences Montpellier (UMR 5243), CNRS, Université Montpellier 2, cc 060, Place E. Bataillon, 34095 Montpellier, France
[c] Laboratoire de Sciences de la Terre (UMR 5570), CNRS, Université Claude Bernard Lyon I, 2 rue Raphaël Dubois, 69622 Villeurbanne, France
[d] Department of Earth Sciences, University of Ottawa, Ottawa, Ontario, Canada, K1N 6N5
[e] Deutsches GeoForschungsZentrum, Section 3.3, Telegrafenberg, 14473 Potsdam, Germany
[f] CRPG, Nancy-Université, CNRS, 15 rue Notre Dame des Pauvres, 54501 Vandoeuvre lès Nancy Cedex, France

ARTICLE INFO

Article history:
Received 24 February 2011
Received in revised form 29 March 2012
Accepted 11 April 2012
Available online 20 April 2012

Editor: L. Reisberg

Keywords:
Serpentinites
Subduction zones
Mantle wedge
Abyssal peridotites
Fluid-mobile elements

ABSTRACT

Serpentinites from subduction environments represent an important sink for fluid-mobile elements. In order to constrain geochemical behavior of fluid-mobile elements hosted by serpentine phases during subduction processes, we carried out a geochemical study (trace elements and Pb isotopes) of a series of serpentinites and cumulates from the accretionary wedge of Greater Caribbean (Cuba and Dominican Republic). The trace element compositions of the primary and alteration-related phases were analyzed in situ using LA–HR-ICP-MS techniques. The studied samples represent parts of the subducted proto-Atlantic oceanic lithosphere, which has experienced low to high grade metamorphism (greenschist to eclogite facies), before being exhumed; a subset of these samples were derived from the mantle wedge. This sampling provides the opportunity to trace the chemical mobility of fluid-mobile elements during prograde metamorphism along a cold geotherm in an oceanic subduction setting.

Serpentinites display strong enrichment in fluid-mobile elements indicating extensive fluid–rock interaction. In situ analyses allow distinction of three types of serpentines related to the nature of primary minerals (olivine, ortho- or clinopyroxene). Compositions of subducted samples, especially in fluid-mobile elements, are relatively close to those of abyssal peridotites without noticeable evidence of mobility for trace elements during subduction-related prograde metamorphism, with the exception of B. This confirms that the observed enrichment results from seawater/peridotite interactions during residence time in the ocean. It also suggests that most mobile elements stored in serpentine minerals are immobile during subduction processes. A major consequence of this observation is that serpentine minerals are a good sink for mobile elements in subduction zones, until their dehydration. Additionally, Pb isotopes and over-enrichment in As–Sb in high-grade subducted serpentines (antigorite) suggest the contribution of a sedimentary component during a secondary hydration taking place at the lizardite/antigorite transition. We propose that this new serpentinization event, taking place at greater depth, results from mixing between sediments and serpentinites in the subduction channel.

Mantle wedge serpentinites present imprints of hydrothermal fluids: they are B-rich but without strong enrichment in As and Sb, and show evidence for moderate contributions of a radiogenic Pb-component. This suggests that the fluids that produced the mantle wedge serpentinites derived from the dehydration of the oceanic crust, with moderate to no contribution of sediments. We posit that mantle wedge serpentinization took place around 20–25 km depth: at such depth and temperature conditions ($T > 200$ °C), the subducted sediments still released their B-rich pore fluids while their structural water incorporated in hydrous minerals (phengite, lawsonite) remained stable. The existence of various potential reservoirs for fluid-mobile elements in subduction zone environments (subducted serpentinites, mantle wedge serpentinites, as well as subducted sediments and altered oceanic crust) that potentially release their fluids at different depths has strong implications for arc lava formation.

1. Introduction

The release of fluids from the downwelling oceanic lithosphere plays an important role during subduction; in particular, it triggers partial melting in the mantle wedge and affects the composition of the arc

* Corresponding author at: Géosciences Montpellier (UMR 5243), CNRS, Université Montpellier 2, cc 060, Place E. Bataillon, 34095 Montpellier, France.
E-mail address: Fabien.Deschamps@gm.univ-montp2.fr (F. Deschamps).

0009-2541/$ – see front matter © 2012 Elsevier B.V. All rights reserved.
doi:10.1016/j.chemgeo.2012.04.009

magmatism and the global geochemical cycles (e.g. Plank and Langmuir, 1998; Stern, 2002; Rüpke et al., 2004; van Keken et al., 2011). Although serpentinized mantle rocks constitute a minor fraction of the downwelling slab, from a few percent (or less) of fast spread lithosphere (Iyer et al., 2010) up to 20% of slow spread lithosphere (Cannat et al., 1995; Carlson, 2001; Mével, 2003), they represent a major reservoir for fluid-mobile elements (FME) in subducting lithosphere at mantle depth (e.g. Scambelluri et al., 2001a,b; Barnes and Straub, 2010; Deschamps et al., 2010, 2011; John et al., 2011). Recent studies of serpentinites sampled at present-day and fossil convergent margins have shown that they can incorporate important quantities of FME, such as semi-volatile elements As and Sb (e.g. Hattori and Guillot, 2003, 2007; Deschamps et al., 2010, 2011), light elements B and Li (e.g. Bonatti et al., 1984; Scambelluri et al., 2004a; Tonarini et al., 2007, 2011; Pabst et al., 2011) and Large Ion Lithophile Elements Cs, Rb, Ba, and U (Scambelluri et al., 2001a,b, 2004b; Tenthorey and Hermann, 2004; Garrido et al., 2005; Savov et al., 2005; Agranier et al., 2007). Further studies have demonstrated that these elements are stored in serpentine phases during prograde metamorphism (Scambelluri et al., 2001a,b, 2004a,b; Deschamps et al., 2011; Kodolányi and Pettke, 2011; Vils et al., 2011), until their destabilization at relatively great depths (>150 km, up to 650–700 °C; Ulmer and Trommsdorff, 1995; Wunder and Schreyer, 1997; Wunder et al., 2001). Finally, strong FME enrichments were observed in high-pressure serpentine minerals (antigorite) sampling the hydrated mantle wedge (e.g. in Himalaya, Hattori and Guillot, 2003, 2007; Deschamps et al., 2010; Mariana forearc, Savov et al., 2005). However, the mechanisms driving the chemical mass transfers from the downwelling slab to the mantle wedge and the sequence of mineralogical reactions controlling the dehydration–hydration processes at depth are still poorly constrained. In addition, little is known about the acquisition of the FME signature during the hydration of mantle wedge and the formation of serpentinites during subduction (e.g. Savov et al., 2005, 2007; Deschamps et al., 2010).

To better understand these processes, we studied a series of serpentinites from Cuba and the Dominican Republic, which sample parts of the accretionary wedge of the Greater Caribbean volcanic arc. These serpentinites are parts of the subducted proto-Atlantic oceanic lithosphere (highly serpentinized peridotites and hydrothermally altered cumulates), and of the hydrated mantle wedge (Hattori and Guillot, 2007; Guillot et al., 2009; Saumur et al., 2010). The subducted and mantle wedge serpentinites are associated in the field, and represent an extinct paleo-serpentinite subduction channel. The slab preserves evidence of low- to high-grade metamorphism (greenschist to eclogite facies). The close association in the field of serpentinites from the mantle wedge and from the subducted oceanic lithosphere provides a unique opportunity to understand the chemical mobility of FME associated with fluid loss during prograde metamorphism along the subduction zone and to characterize geochemical transfers from the slab to the overlying mantle wedge peridotite.

In order to constrain the behavior of the fluid-mobile elements hosted by serpentine minerals during subduction, we carried out in situ trace element analyses on serpentine phases and associated minerals from subducted and mantle wedge serpentinites as well as measurements of Pb isotope compositions for Cuban samples. These data are used to characterize the nature of the protolith and of hydrating fluid(s) in the slab and in the mantle wedge and to discuss the role of serpentinization and dehydration in the cycling of FME during prograde metamorphism associated with intra-oceanic subduction processes.

2. Geological setting and sampling

The Dominican Republic and Cuba are part of the extinct Greater Caribbean volcanic arc, which marks the northern margin of the Caribbean plate (Fig. 1a). The Greater Caribbean arc results from the eastward subduction of the Farallon plate at the southern margin of the North American plate during Cretaceous (Pindell et al., 2005). By mid-Cretaceous, the polarity of subduction changed and caused the migration of the arc from the Pacific to the Atlantic side and the divergence between North and South America, which was accommodated by rifting of the proto-Caribbean ridge (Pindell et al., 1988; Meschede and Frisch, 1998).

Well preserved ophiolitic terranes outcrop in the northern part of Cuba (Escambray massif and Zaza zone; Fig. 1b) and in the Dominican Republic (Rio San Juan complex; Fig. 1c). They are characterized by abundant serpentinites associated with metamorphic rocks, making these massifs particularly interesting for studying serpentinites in convergent settings, as the metamorphic conditions experienced by the selected samples could be deduced from the associated metamorphic rocks. For this geochemical study, we selected 15 samples from serpentinite series that had already been well characterized in terms of geodynamic setting, petrography and bulk-rock geochemistry (Cuba: Auzende et al., 2002; Hattori and Guillot, 2007; Dominican Republic: Saumur et al., 2010).

2.1. Cuba

The island of Cuba is composed of a series of accreted terranes of continental and oceanic origins, all younger than Jurassic (Iturralde-Vinent, 1994). The Zaza zone and Escambray massif belong to the central Cuba unit (Meyerhoff and Hatten, 1968; Fig. 1b). The Zaza zone is an allochtonous oceanic unit located north of a thick sequence comprising Cretaceous volcanic arc and sedimentary rocks (noted Cretaceous arc on Fig. 1b). It consists of a mélange of lenses of eclogitic basalts and gabbros associated with strongly deformed serpentinites (Piotrowska, 1993). They represent the relics of an accretionary prism developed during the southward subduction of the proto-Caribbean oceanic plate (Pindell et al., 1988). Locally, the transition from the Zaza zone to the Cretaceous arc sequence is marked by a highly deformed area, which preserves parts of the mantle wedge. Located to the SW of the Zaza zone and of the Cretaceous arc sequence (Fig. 1b), the Escambray massif is composed mainly of lenses of serpentinites (several hundred meters in length) associated with metasedimentary rocks and metamorphosed basalts (Schneider et al., 2004; Stanek et al., 2006). It is interpreted as an old accretionary prism formed in a forearc setting in the Greater Caribbean Arc (Somin and Millán, 1981; Burke, 1988; Millán, 1997; Iturralde-Vinent, 1998; Pindell et al., 2005; García-Casco et al., 2008). Six serpentinites and two altered ultramafic cumulates were selected for this study; these samples were previously described by Auzende et al. (2002) and Hattori and Guillot (2007) and their main characteristics are summarized below.

Three serpentinites (CU 54, CU 55, CU 56) and one ultramafic cumulate (CU 62) were sampled in the Zaza zone. Samples CU 55, CU 56 and CU 62 are associated in the field with metabasic rocks characterized by a low-pressure amphibolitic assemblage (<0.6 GPa, 400–500 °C; Spear, 1993; Auzende et al., 2002). In contrast, sample CU 54 is associated with basalts metamorphosed under higher temperature conditions in the amphibolite/eclogite metamorphic facies (>0.3 GPa, >500 °C; Spear, 1993; Auzende et al., 2002). Serpentinite CU 63 was sampled in the deformation zone set between the Zaza zone and the base of the Cretaceous arc sequence, close to the city of Santa Clara. It is associated with greenish gabbros (<0.6 GPa, 300–400 °C; Auzende et al., 2002). It is interpreted as sampling the hydrated mantle wedge (Hattori and Guillot, 2007). Finally, two serpentinites (CU 24 and CU 65) and one altered ultramafic cumulates (CU 69) were sampled in the Escambray massif. Serpentinites CU 24 and CU 65 are associated with high pressure rocks which have experienced metamorphic conditions in the zoisite-eclogitic facies (1.5–1.6 GPa, 600–650 °C; Schneider et al., 2004; Stanek et al., 2006; Garciá-Casco et al., 2006) and sample CU 69 comes from the greenschist facies nappe (0.7–0.8 GPa, <500 °C; Schneider et al., 2004).

The Cuban serpentinites comprise either antigorite (CU 24, CU 54 and CU 65) or an assemblage of fine-grained lizardite and chrysotile

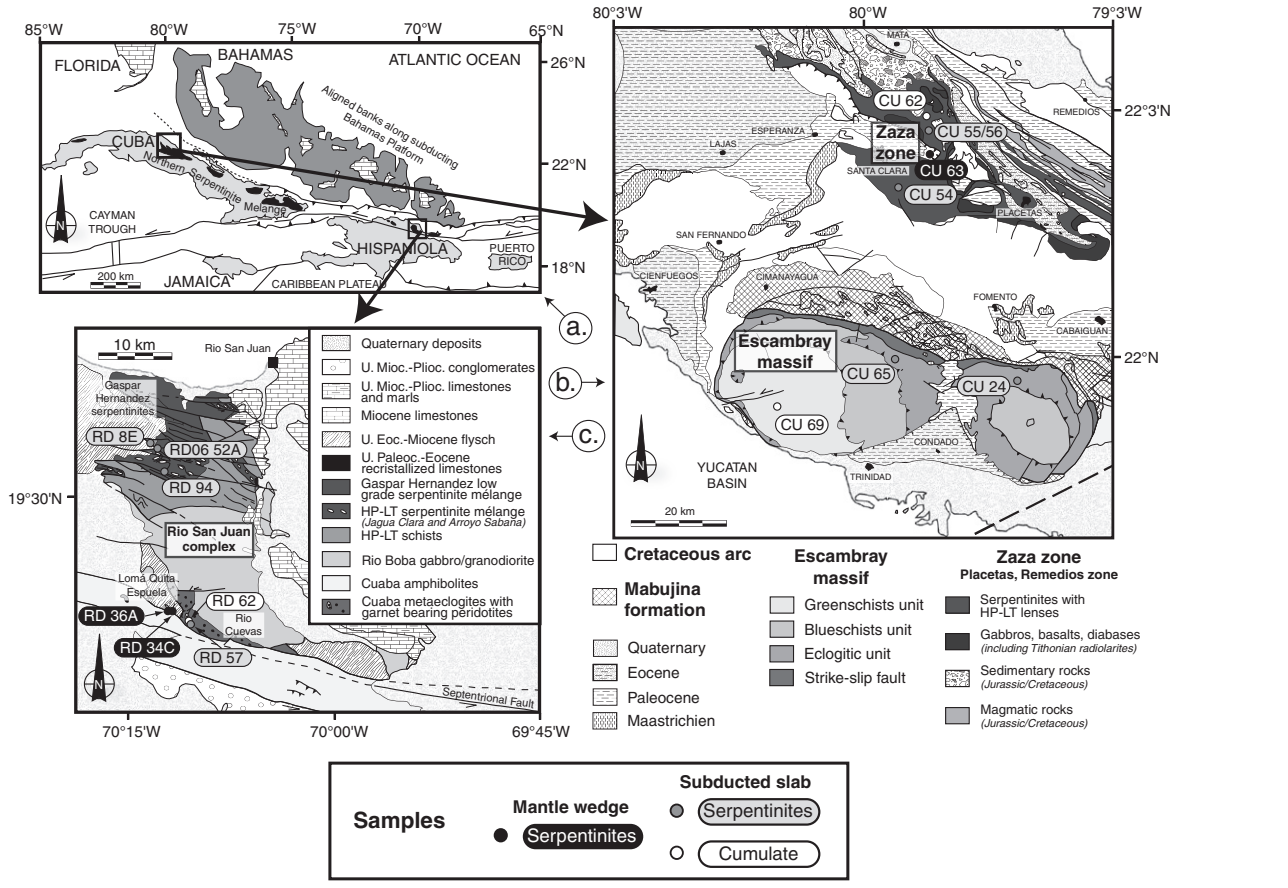

Fig. 1. a) General map of the northeastern Caribbean area showing the main inliers of subduction complex with outcrop of serpentinites (black zone) in Cuba and Dominican Republic (redraw after Dolan et al., 1998; Saumur et al., 2010).b) Geological map of the central part of Cuba with location of studied serpentinites (redraw after Millan, 1993; Auzende et al., 2002).c) Geological map of the Rio San Juan complex in Dominican Republic (Hispaniola Island) with location of studied serpentinites (map was modified from Lewis et al., 1990; Mann et al., 1991; Pindell and Draper, 1991; Draper and Nagle, 1991; Abbott et al., 2006; Saumur et al., 2010).Gray and white circles represent the serpentinites and cumulate, respectively, sampling the subducted oceanic lithosphere, and the solid circles represent serpentinites from the mantle wedge.

(CU 55, CU 56 and CU 63) as distinguished by X-ray diffraction and previous work (Raman spectroscopy, Hattori and Guillot, 2007), plus minor disseminated magnetite, talc, edenite (CU 65), and chlorite (clinochlore in CU 54 and CU 56; Table 1). Lizardite-bearing samples CU 56 and CU 63 are characterized by pseudomorphic hourglass textures (preserving the shape of the primary grains). Antigorite-bearing samples CU 54 and CU 65 have non-pseudomorphic textures dominated by penetrative blades of antigorite. The two ultramafic cumulates CU 62 and CU 69 are composed mostly of tremolite, edenite, chlorite and talc.

2.2. Dominican Republic

Dominican serpentinites come from the Rio San Juan Complex (RSJC), located in the northern part of the Dominican Republic (NE margin of Hispaniola; Fig. 1c). This complex is mostly covered by sedimentary rocks from Miocene to Quaternary (Draper and Nagle, 1991). It is subdivided into three parts: the Gaspar Hernandez serpentinites in the north, metamorphic terranes mainly composed of retrogressed blueschists and eclogites in the central part, and the Cuaba Gneiss and the Rio Boba Gabbro in the South. The central part of RSJC is intruded by two serpentinite mélanges, the Jagua Clara mélange and the Arroyo Sabana mélange. They represent tectonic mélanges containing meter-scale blocks of blueschists (peak metamorphism at 1.7–1.8 GPa/340–380 °C), eclogites (2.3 GPa/750 °C; Krebs et al., 2008), metamorphosed felsic rocks and serpentinites from subducted slab. Finally, massive boulders of serpentinites outcrop in the southern part of RSJC, near the intersection between the Septentrional Fault Zone and the Bajabonico Fault in Lomá Quita Espuela and Rio Cuevas. These serpentinites represent the remnants of the subducted oceanic lithosphere; they are associated with garnet peridotites and eclogite boulders. Locally, mantle wedge serpentinites occur along major strike–slip fault and are associated with the subducted serpentinites (Saumur et al., 2010). Seven serpentinites were selected for this study among those described by Saumur et al. (2010); their main characteristics are summarized below.

Three serpentinites (RD 8E, RD 94, and RD06 52A) were collected in the high pressure–low temperature Jagua Clara mélange in the central part of the RSJC (Fig. 1c). The four remaining samples come from a large outcrop in the southern part of RSJC near the Septentrional Fault Zone (Fig. 1c). Serpentinites RD 34C and RD 36A come from the Lomá Quita Espuela area and represent relics of the hydrated mantle wedge. One partially hydrated peridotite (RD 57) and one hydrated cumulate (RD 62) were sampled in Rio Cuevas area and represent part of the ancient subducted lithosphere.

Dominican serpentinites comprise mainly antigorite (RD 8E and RD06 52A) or an assemblage of lizardite/chrysotile (RD 34C, RD 36A and RD 94), with minor magnetite, chromite, hematite, talc, chlorite (clinochlore), and amphibole (edenite, magnesio-hornblende; Table 1). Several samples contain relics of primary olivines (RD 94) and pyroxenes (RD 36A, RD06 52A and RD 94). One sample, RD 57, is significantly less altered than associated serpentinites; it comprises mainly forsterite-rich olivine and diopside displaying secondary alteration to lizardite, edenite, magnesio-hornblende and clinochlore. This sample is representative of a partially hydrated peridotite (less than 10% of hydrated phases). The hydrated cumulate RD 62 comprises mainly diopside and hornblende.

Table 1
Mineralogy and bulk rock major element compositions of samples from Cuba and Dominican Republic. (n.d. = not determined). Major elements are compiled from Hattori and Guillot (2007; Cuba) and Saumur et al. (2010; Dominican Republic) (see footnotes for more details, notably about analytical method).

Sample	CU 56	CU 54	CU 65	CU 62	CU 63	RD 94	RD 57	RD 8E	RD06 52A	RD 62	RD 34C	RD 36A
Rock[a]	Serp.	Serp.	Serp.	Hydr. cum.	Serp.	Serp.	Hydr. per.	Serp.	Serp.	Hydr. cum.	Serp.	Serp.
Location[b]	Zaza	Zaza	Escambray	Zaza	Def. Zone	melange	SFZ-RC	melange	melange	SFZ-RC	SFZ-LQE	SFZ-LQE
Protolith[c]	Oceanic Lithosphere	Oceanic Lithosphere	Oceanic Lithosphere	Oceanic Cumulate	Mantle Wedge	Oceanic Lithosphere	Oceanic Lithosphere	Oceanic Lithosphere	Oceanic Lithosphere	Oceanic Cumulate	Mantle Wedge	Mantle Wedge
Group[d]	1a	1b	1b	2	3	1a	1a	1b	1b	2	3	3
	(Hattori and Guillot, 2007)					(Saumur et al., 2010)						
SiO_2	38.88	42.21	41.17	43.52	39.71	44.72	41.18	39.3	42.31	43.68	39.84	40.84
TiO_2	0.049	0.039	0.018	0.017	0.009	0.047	0.077	0.020	0.108	0.608	0.021	0.022
Al_2O_3	2.15	1.74	3.01	7.68	0.57	2.51	1.63	1.60	1.16	13.36	0.70	0.69
$Fe_2O_{3\ (t)}$	9.15	8.21	9.74	7.16	8.22	8.14	13.25	10.03	9.89	10.67	8.75	8.60
MnO	0.096	0.115	0.121	0.094	0.093	0.119	0.189	0.060	0.120	0.182	0.118	0.086
MgO	35.43	35.34	34.04	26.83	36.87	34.98	32.89	37.00	33.94	15.95	38.02	37.25
CaO	0.10	0.06	0.08	5.60	0.05	0.18	6.51	0.06	3.19	11.97	0.48	0.39
Na_2O	n.d.	n.d.	n.d.	0.34	n.d.	n.d.	n.d.	n.d.	n.d.	0.87	n.d.	n.d.
K_2O	n.d.	n.d.	n.d.	0.04	0	n.d.	0.02	n.d.	0	0.33	n.d.	0
P_2O_5	0.005	0.004	0.004	0.008	0.008	0.020	0.010	0.010	0.010	0.100	0.010	0.010
L.O.I.	13.7	11.9	12.3	8.1	14.0	10.0	4.6	12.7	9.9	1.5	13.1	13.6
Mg/Si	1.18	1.08	1.07	0.80	1.20	1.01	1.03	1.21	1.03	0.47	1.23	1.18
Al/Si	0.06	0.05	0.08	0.20	0.02	0.06	0.04	0.05	0.03	0.35	0.02	0.02
Mineralogy[e]	(determined by petrographical observations and associated microprobe analysis)											
Serpentine:	Lz, Ctl	Atg	Atg	–	Lz, Ctl	Lz, Ctl	Lz	Atg	Atg	–	Lz, Ctl	Lz, Ctl
After Ol	–	√	–	–	√	√	√	–	√	–	√	√
After Opx	–	√	–	–	–	√	–	√	√	–	–	√
After Cpx	√	–	√	–	–	–	√	√	√	–	–	–
Olivine:	–	–	–	–	–	√	Forsterite	–	–	–	–	–
Pyroxene:	–	–	–	–	–	Enstatite	Diopside	–	Augite	Diopside	–	Enstatite
Amphibole:	–	–	Ed	Ed, Tr	–	Ed, Mg-Hbl	Ed, Mg-Hbl	–	–	Hbl	Ed, Mg-Hbl	–
Chlorite:	Clinochlore	Clinochlore	–	√	–	Clinochlore	Clinochlore	Clinochlore	Clinochlore	–	Clinochlore	√
Talc:	–	√	√	√	–	√	–	√	–	–	√	–
Iron oxide:	Mag	–	–	–	Mag	Mag, Chr	Mag	Mag, Chr	Hematite	–	Mag, Chr	Mag, Chr
Calcite:	–	–	–	–	–	–	√	√	√	–	–	–
P–T cond.[f]	<0.6 GPa ≈450 °C	>0.3 GPa >500 °C	1.5–1.6 GPa >600 °C	<0.6 GPa ≈450 °C	<0.6 GPa 300–400 °C	1.6–1.8 GPa 340–380 °C	– –	2.3 GPa 750 °C	2.3 GPa 750 °C	– –	Along a Fault	Along a Fault

Major element concentrations were previously determined and published by Hattori and Guillot (2007; Cuba) and Saumur et al. (2010; Dominican Republic, except samples RD 57 and RD 62, personnal communication) using a Philips PW 2400 X-ray fluorescent spectrometer at the University of Ottawa.

[a] Rock: Serp = serpentinites; Hydr. cum. = hydrated cumulate; Hydr. per. = hydrated peridotites.

[b] Location: Cuba: Zaza = Zaza zone; Escambray = Escambray massif; Def. Zone = major deformation zone; Dominican Republic: Mélange = HP-LT serpentinites Jagua Clara mélange from central part of Rio San Juan complex; SFZ-LQE = Septentrional fault zone, Loma Quita Espuela; SFZ-RC = Septentrional fault zone, Rio Cuevas (see text for details).

[c] Protolith: Oceanic lithosphere = abyssal peridotites; Oceanic cumulate = abyssal cumulative hydrated rocks; Mantle wedge = forearc mantle wedge peridotites.

[d] Group: 1a = Lz-bearing serpentinites and, 1b = Atg-bearing serpentinites of the subducting slab; 2 = Cumulates of the subducting slab; 3 = Atg-bearing mantle wedge serpentinites.

[e] Mineralogy: Atg = antigorite; Lz = lizardite; Ctl = chrysotile; Ed = edenite; Tr = tremolite; Mg-Hbl = magnesio-hornblende; Hbl = hornblende; Mag = magnetite; Chr = chromite (Kretz, 1983).

[f] P–T conditions: Metamorphic conditions experienced by studied serpentinites can be constrained using the associated metamorphic rocks which are well characterized. Cuba: Spear (1993), Auzende et al. (2002), Schneider et al. (2004), Stanek et al. (2006), and Garciá-Casco et al. (2006). Dominican Republic: Krebs et al. (2008). See text for explanations.

2.3. Main petrographic and geochemical characteristics of studied samples

On the basis of the petrographic study and of the mineral and bulk rock major element compositions determined by Hattori and Guillot (2007) and Saumur et al. (2010), we divided the studied samples into four groups (see Table 1):

- (1) *Subducted serpentinites*: subducted serpentinites sample relics of the subducted oceanic lithosphere. They comprise both lizardite-bearing (*CU 55*, *CU 56*, *RD 94*, *RD 57*: *Group 1a*) and antigorite-bearing (*CU 24*, *CU 54*, *CU 65*, *RD 8E*, *RD06 52A*: *Group 1b*) samples indicating different P–T conditions during their formation. Group 1b serpentinites recorded processes occurring at deeper depths than Group 1a serpentinites. The two groups overlap in composition for bulk and mineral major element contents. Subducted serpentinites are characterized by loss on ignition (LOI) ranging from 9.9 to 13.7 wt.% (except sample RD 57, a serpentinized peridotite with 4.6 wt.% LOI), moderate to high Al_2O_3 and CaO contents (1.16–3.01 wt.% and 0.06–6.51 wt.%, respectively), and low to moderate Cr# (0.2–0.55) in spinels. These compositions reflect a fertile mantle protolith, with late addition of magmatic components (CaO > PM values (4 wt.%) in sample RD 57). They are comparable to abyssal peridotites (e.g., Bodinier and Godard, 2003 (bulk); Niu, 2004 (bulk); Dick and Bullen, 1984; Dick, 1989 (spinels)).
- (2) *Subducted cumulates* (*CU 62*, *CU 69*, *RD 62*): these samples represent part of the subducted slab. They are characterized by variable LOI (1.5–8.1 wt.%), high Al_2O_3 (7.68–13.36 wt.%) and CaO (5.60–11.97 wt.%) contents. They are mainly composed of amphiboles, and minor chlorites and primary pyroxenes.
- (3) *Mantle wedge serpentinites* (*CU 63*, *RD 34C*, *RD 36A*): the third group is characterized by lizardite-bearing samples, higher LOI (13.1–14 wt.%), lower Al_2O_3 content (0.57–0.70 wt.%) and higher Cr# spinels (0.50–0.66; Saumur et al., 2010) compared to subducted serpentinites. These compositions indicate a more refractory mantle protolith compared to the protolith of the subducted serpentinites. Mantle wedge serpentinites overlap in composition with the Mariana forearc peridotites (Ishii et al., 1992). We assume that hanging-plate peridotites comprise exclusively highly refractory peridotites, whereas oceanic lithosphere has generally mildly to moderately refractory compositions.

Associated with serpentine, we note the presence of rare chlorite, talc, and amphiboles (edenite, Mg-hornblende) in all Caribbean samples. This observation is consistent with the interpretation that these samples have experienced medium-grade metamorphism (greenschist–blueschist to amphibolite facies; Evans, 1977) during their subduction. Note that no metamorphic olivine has been observed in the studied samples.

3. Analytical procedure

A fraction of each sample was crushed first into small fragments and then reduced to powder in an agate ring mill. Bulk rock major element compositions were published in Hattori and Guillot (2007; Cuban samples), and in Saumur et al. (2010; Dominican samples) with exception of samples RD 57 and RD 62. Complementary bulk rock trace element data were acquired using the same ICP-MS instrument on which in situ trace element compositions were obtained.

3.1. Bulk rock trace element analyses

Trace element concentrations (Li, Cd, Co, Ni, Cu, As, Rb, Sr, Y, Zr, Nb, Cs, Ba, Rare Earth Elements (REE), Hf, Ta, Pb, Th, U and W) were determined at Géosciences Montpellier (University Montpellier 2, France) using a ThermoFinnigan Element2 High Resolution (HR-) ICP-MS. These analyses were obtained together with those reported by Deschamps et al. (2010); the analytical procedure, the detection limits and procedural blanks as well as the precision and accuracy of the ICP-MS analyses are described in detail in this paper. Most elements were measured in low resolution mode ($m/\Delta m \sim 400$), except Co, Ni, and Cu that were analyzed in medium resolution mode ($m/\Delta m \sim 4000$) and As, measured in high resolution mode ($m/\Delta m \sim 10000$). Our results show good agreement between measured values and expected values for the international rock standards (dunite DTS-1, peridotite JP-1 and serpentinite UBN), and reproducibility is generally better than 1% at concentrations >1 μg/g; it is within 1–5% for concentrations of 0.01–1 μg/g, and 5–10% for concentrations less than 0.01 μg/g. Results of trace element analyses for Cuban and Dominican serpentinites are reported in Table 2.

3.2. Lead isotopes

The Pb chemistry was done at LGCA (University of Grenoble, France), using the anion resin technique of Manhès et al. (1984), while the isotopic ratios were measured using the MC -ICP-MS national facility at Ecole Normale Supérieure (ENS) of Lyon (France). The method for Pb elution is described in Chauvel et al. (2011). Procedural blank was negligible (<50 pg; n = 2) relative to the amounts of Pb in samples and blank correction was therefore not applied. The NBS 981 standard was run every second sample and Pb isotope ratios were corrected by sample-standard bracketing to the NBS 981 TIMS values (Galer and Abouchami, 1998). Due to fluid circulation during serpentinization, we cannot consider hydrated peridotites as a closed system; so no age corrections were applied to our samples. Results are reported in Table 3.

3.3. Mineral characterization

The mineralogy of bulk samples was characterized using a Siemens D5000 X-ray diffractometer at LGIT (Grenoble, France). A Cameca SX 100 electron microprobe at the Laboratory Magma et Volcans (Clermont Ferrand, France) was used to determine the major element concentrations of minerals. The operating conditions were 15 kV accelerating voltage, sample current of 15 nA and count time of 10 s/element, except for Ni (20 s). Standards used were albite (Na), forsterite (Mg), orthose (K), wollastonite (Ca and Si), $MnTiO_3$ (Ti and Mn), Cr_2O_3 (Cr), fayalite (Fe), olivine (Ni), and synthetic Al_2O_3 (Al).

In situ trace element compositions were determined at Géosciences Montpellier (University Montpellier 2, France) using a ThermoFinnigan Element 2 HR-ICP-MS using a single collector double-focusing sector field Element XR (eXtended Range) coupled with laser ablation (LA) system, a Geolas (Microlas) automated platform housing a 193 nm Compex 102 laser from LambdaPhysik. Analyses were carried out on 150 μm thick polished sections using the method, settings and calibration techniques described in Deschamps et al. (2010). A spot size of 77 μm was used for sample CU 54, and 122 μm for other samples. A large beam size was used during this study to achieve better accuracy. This resulted in a sensitivity of ~500 cps/ppm for B, of ~2000 cps/ppm for Li, Ni, Ti, Zn, As and Cr, and of ~18,000 cps/ppm for the other analyzed elements based on measurements of the NIST 612 certified reference material. Data were subsequently reduced using the GLITTER software (Van Achterberg et al., 2001) using the linear fit to ratio method. This typically resulted in a 5 to 10% precision (1 sigma) for most analyses evaluated by repeated analyses of reference basalt BIR 1-G (values are reported in Deschamps et al., 2010; preferred values from Jochum et al., 2005; Jochum and Stoll, 2008). Detection limits were below 0.08 μg/g for most elements except Li (average of ~0.8 μg/g), B (~0.6 μg/g), Ti (~5 μg/g), Cr (~3 μg/g), Ni (~25 μg/g), Zn (~2 μg/g) and As (~0.3 μg/g). Values within 2σ of the detection limit were eliminated using a logical test ((values -2σ) > detection limit). Representative trace element analyses are reported in Table 4; all results are reported in Appendices 1 (serpentine phases) and 2 (amphiboles, chlorites, iron oxides).

To minimize the contribution of other phases, we analyzed homogeneous clear areas with characteristic habitus of lizardite, chrysotile, and antigorite, in the limit of apparatus optical resolution. However, we cannot preclude that some serpentine phases contain dusty inclusions of magnetite and other minor secondary phases (chlorite, calcite, sulfide) which may concentrate certain trace elements (e.g. Ti in magnetite or As and Sb in sulfides). We tried to limit the possible influence of such grains during analysis using GLITTER software, which displays elementary ablation profile, and thus allows elimination of contaminated and/or mixed analyses.

4. Results

4.1. Bulk rock trace element compositions

The subducted serpentinites (Group 1) have moderately depleted compositions with MREE and HREE compositions and ratios close to C1-chondrite values (e.g. $Yb_N = 0.67–1.28$; $Gd_N/Yb_N = 0.60–1.38$; $_N$ = C1-chondrite normalized; Fig. 2a, b). Group 1 serpentinites are LREE depleted relative to MREE and HREE ($La_N/Sm_N \approx 0.25$), except for samples CU 54 and RD 94 which display selective enrichments in LREE ($La_N/Sm_N = 1.33–2.45$). Group 1 serpentinites are characterized by variable Eu anomalies, from slightly positive (RD 57, $Eu_N/Eu^*_N = 1.23$) to none in the Dominican serpentinites ($0.80 < Eu_N/Eu^*_N < 1.00$) to negative ($0.60 < Eu_N/Eu^*_N < 0.79$) in the Cuban serpentinites and Dominican serpentinites RD 8E. Except for the Eu anomalies, the REE composition of Group 1 serpentinites is comparable to that of the lherzolites sampled in the Western Alps ophiolites (see review in Bodinier and Godard, 2003) for the LREE depleted samples. Group 1 serpentinites plot in the field defined by Paulick et al. (2006) for the impregnated abyssal peridotites (Fig. 2c).

Cumulate CU 62 (Group 2) has higher REE contents compared to serpentinites (e.g., Yb_N ~3; Fig. 2a). It is characterized by a convex-upward REE pattern with a strong depletion in LREE ($La_N/Sm_N = 0.11$), similar to that of spinel pyroxenites in orogenic massifs (e.g., Bodinier and Godard, 2003). Similar to Group 1 serpentinites, it displays a strong negative Eu anomaly ($Eu_N/Eu^*_N = 0.37$).

In contrast, mantle wedge serpentinites (Group 3) are characterized by low HREE contents (e.g., $Yb_N = 0.19–0.29$) and by enrichment in LREE relative to MREE and even HREE in sample RD 34C ($Gd_N/Yb_N = 0.31–0.98$; $La_N/Yb_N = 0.62–2.34$; Fig. 2a, b). These selective LREE enrichment are commonly interpreted as the result of progressive melt/rock reequilibration associated with the percolation of LREE-rich melts infiltrating a depleted mantle (e.g. Navon and Stolper, 1987; Bodinier et al., 1990; Bodinier and Godard, 2003). Group 3 samples display no to slight Eu anomalies ($Eu_N/Eu^*_N = 1.06–1.19$). Their composition is typical of forearc serpentinites (Savov et al., 2005, 2007; Deschamps et al., 2010; Fig. 2c).

Table 2
Bulk rock trace element (HR-ICP-MS) concentrations (in μg/g) for Cuban and Dominican serpentinites. (n.d. = not determined). Errors are given at the 2σ level (in μg/g).

Sample	CU 54	2σ error	CU 56	2σ error	CU 65	2σ error	CU 62	2σ error	CU 63	2σ error
Group	1b		1a		1b		2		3	
		(μg/g)		(μg/g)		(μg/g)		(μg/g)		(μg/g)
Li (μg/g)	2.79	0.0003	0.96	0.0001	n.d.	n.d.	n.d.	n.d.	0.66	0.0001
Co	84	0.0041	121	0.0080	107	0.0098	87	0.0035	119	0.0061
Ni	1570	0.0900	2358	0.1108	2114	0.0415	1715	0.0157	3603	0.0449
Cu	14.0	0.0007	25.8	0.0013	60.3	0.0015	3.1	0.0002	3.8	0.0003
As	3.74	0.0003	0.34	0.0002	0.64	0.0006	0.64	0.0005	0.19	0.0001
Rb	0.09	0.0096	0.06	0.0041	0.04	0.0055	0.239	0.0065	0.13	0.0062
Sr	3.95	0.1010	1.11	0.0374	0.61	0.0557	21.117	0.6831	2.08	0.0189
Y	0.891	0.0268	0.973	0.0173	1.032	0.0131	4.892	0.1139	0.128	0.0028
Zr	0.318	0.0033	0.473	0.0129	0.322	0.0163	0.558	0.0422	0.140	0.0052
Nb	0.129	0.0081	0.011	0.0013	0.092	0.0165	0.020	0.0015	0.006	0.0014
Cd	0.03	0.0000	0.02	0.0000	0.04	0.0000	0.07	0.0000	0.06	0.0000
Cs	0.020	0.0004	0.012	0.0007	0.012	0.0019	0.014	0.0010	0.011	0.0037
Ba	29.200	0.1395	0.735	0.0539	0.708	0.0329	1.427	0.0440	2.453	0.0791
La	0.3382	0.0043	0.0202	0.0011	0.0310	0.0016	0.0697	0.0014	0.0273	0.0019
Ce	0.9326	0.0213	0.0432	0.0018	0.1120	0.0023	0.3531	0.0128	0.0644	0.0012
Pr	0.1309	0.0027	0.0096	0.0007	0.0232	0.0007	0.0979	0.0026	0.0090	0.0012
Nd	0.5850	0.0237	0.0853	0.0016	0.1434	0.0070	0.7546	0.0023	0.0386	0.0038
Sm	0.1588	0.0109	0.0515	0.0020	0.0664	0.0105	0.3904	0.0041	0.0093	0.0024
Eu	0.0340	0.0011	0.0203	0.0016	0.0185	0.0009	0.0650	0.0010	0.0040	0.0004
Gd	0.1808	0.0130	0.1117	0.0099	0.1258	0.0114	0.7282	0.0262	0.0114	0.0006
Tb	0.0280	0.0016	0.0218	0.0005	0.0268	0.0005	0.1412	0.0009	0.0022	0.0002
Dy	0.1808	0.0114	0.1706	0.0150	0.2068	0.0099	1.0284	0.0245	0.0195	0.0040
Ho	0.0349	0.0017	0.0390	0.0015	0.0444	0.0015	0.2095	0.0015	0.0049	0.0004
Er	0.1053	0.0065	0.1169	0.0011	0.1344	0.0019	0.5618	0.0176	0.0175	0.0020
Tm	0.0165	0.0009	0.0194	0.0009	0.0225	0.0003	0.0792	0.0022	0.0037	0.0002
Yb	0.1091	0.0070	0.1356	0.0091	0.1685	0.0011	0.4575	0.0099	0.0299	0.0040
Lu	0.0180	0.0011	0.0252	0.0006	0.0299	0.0006	0.0687	0.0024	0.0061	0.0007
Hf	0.0151	0.0026	0.0221	0.0033	0.0175	0.0032	0.0412	0.0020	0.0040	0.0022
Ta	0.0060	0.0004	0.0002	0.0001	n.d.	n.d.	0.0015	0.0001	0.0001	0.0000
W	n.d.	n.d.	0.014	0.0000	n.d.	n.d.	n.d.	n.d.	0.003	0.0000
Pb	n.d.	n.d.	0.264	0.0055	0.283	0.0204	0.603	0.0234	0.623	0.0048
Th	0.251	0.0088	0.008	0.0010	0.028	0.0002	0.019	0.0008	0.011	0.0016
U	0.073	0.0031	0.135	0.0028	0.248	0.0028	0.056	0.0011	0.017	0.0017

Sample	RD 8E	2σ error	RD 94	2σ error	RD06 52A	2σ error	RD 34C	2σ error	RD 57	2σ error
Group	1b		1a		1b		3		1a	
		(μg/g)		(μg/g)		(μg/g)		(μg/g)		(μg/g)
Li (μg/g)	n.d.	n.d.	n.d.	n.d.	1.92	0.0002	n.d.	n.d.	2.01	0.0001
Co	109	0.0069	105	0.0069	133	0.0044	123	0.0023	129	0.0148
Ni	2108	0.1338	2132	0.0523	1399	0.0732	2221	0.0601	516	0.0159
Cu	9.9	0.0009	5.2	0.0005	3.3	0.0001	1.4	0.0001	7.5	0.0004
As	1.52	0.0005	0.31	0.0004	1.70	0.0016	0.22	0.0001	0.64	0.0007
Rb	0.04	0.0040	0.08	0.0034	0.04	0.0024	0.09	0.0056	0.59	0.0241
Sr	15.99	0.8315	3.84	0.1279	5.73	0.1041	16.46	0.3818	16.64	0.1913
Y	0.964	0.0386	1.680	0.0330	1.683	0.0328	0.279	0.0130	1.061	0.0206
Zr	0.285	0.0138	0.591	0.0177	1.600	0.0257	0.239	0.0017	0.433	0.0045
Nb	n.d.	n.d.	0.029	0.0012	0.010	0.0006	n.d.	n.d.	0.006	0.0008
Cd	0.01	0.0000	0.05	0.0000	0.08	0.0000	0.01	0.0000	0.04	0.0000
Cs	0.012	0.0041	0.088	0.0049	0.008	0.0010	0.077	0.0018	0.036	0.0042
Ba	0.441	0.0572	16.488	0.4368	1.706	0.0500	22.112	0.5986	11.672	0.2122
La	0.0188	0.0010	0.4027	0.0067	0.0540	0.0011	0.1590	0.0049	0.0429	0.0033
Ce	0.0932	0.0043	0.1608	0.0006	0.1472	0.0068	0.3994	0.0013	0.1210	0.0035
Pr	0.0218	0.0011	0.0930	0.0040	0.0382	0.0022	0.0508	0.0011	0.0236	0.0015
Nd	0.1546	0.0069	0.4725	0.0031	0.2808	0.0051	0.2158	0.0059	0.1667	0.0040
Sm	0.0718	0.0042	0.1025	0.0128	0.1357	0.0120	0.0478	0.0044	0.0878	0.0050
Eu	0.0195	0.0011	0.0373	0.0026	0.0580	0.0016	0.0181	0.0007	0.0500	0.0011
Gd	0.1331	0.0033	0.1866	0.0024	0.2281	0.0087	0.0557	0.0029	0.1691	0.0031
Tb	0.0263	0.0007	0.0259	0.0015	0.0438	0.0024	0.0080	0.0001	0.0303	0.0010
Dy	0.1954	0.0070	0.1631	0.0034	0.3256	0.0057	0.0473	0.0004	0.2266	0.0054
Ho	0.0430	0.0020	0.0370	0.0014	0.0714	0.0009	0.0099	0.0002	0.0474	0.0013
Er	0.1252	0.0067	0.1110	0.0040	0.2044	0.0036	0.0339	0.0018	0.1338	0.0115
Tm	0.0198	0.0014	0.0160	0.0008	0.0309	0.0004	0.0056	0.0003	0.0185	0.0006
Yb	0.1284	0.0034	0.1090	0.0046	0.2074	0.0013	0.0461	0.0010	0.1167	0.0014
Lu	0.0228	0.0015	0.0242	0.0011	0.0338	0.0008	0.0096	0.0003	0.0201	0.0015
Hf	0.0244	0.0023	0.0214	0.0017	0.0757	0.0044	0.0051	0.0005	0.0204	0.0029
Ta	n.d.	n.d.	0.0014	0.0005	0.0009	0.0007	0.0030	0.0002	0.0002	0.0001
W	n.d.	n.d.	n.d.	n.d.	0.025	0.0000	n.d.	n.d.	n.d.	n.d.
Pb	1.360	0.0378	0.331	0.0251	0.063	0.0038	0.810	0.0429	0.884	0.0206
Th	0.002	0.0002	0.011	0.0012	0.002	0.0007	0.061	0.0011	0.002	0.0009
U	0.019	0.0006	0.009	0.0001	0.042	0.0008	0.041	0.0014	0.008	0.0008

Table 3
Pb isotopic compositions for Cuban serpentinites. Errors are given at the 2σ level. *Bis* are for duplicate dissolution and *Rep* for duplicate run.

Sample		$^{206}Pb/^{204}Pb$	±2σ	$^{207}Pb/^{204}Pb$	±2σ	$^{208}Pb/^{204}Pb$	±2σ
CU 24	(Group 1b)	18.7524	±15	15.6599	±13	38.3040	±33
CU 55	(Group 1a)	17.8845	±08	15.5800	±09	37.5710	±24
CU 62	(Group 2)	18.5567	±13	15.6461	±14	38.2301	±34
CU 62 (Bis)	(Group 1b)	18.5595	±10	15.6471	±08	38.2358	±24
CU 63	(Group 3)	18.1494	±15	15.6179	±15	38.0464	±39
CU 65	(Group 1b)	19.0177	±28	15.6718	±22	38.4549	±56
CU 69	(Group 2)	18.6606	±12	15.6532	±10	38.5552	±28
CU 69 (Rep)	(Group 2)	18.6595	±17	15.6534	±14	38.5677	±53
MC–ICP-MS standards							
NBS 981							
Galer and Abouchami (1998)		16.94	±15	15.5	±16	36.72	±44
Average (n = 11)		16.9395	±330	15.4892	±174	36.6968	±224
Biais (μg/g)		60		459		683	

As shown in Fig. 2d and e, the serpentinite trace element compositions normalized to Primitive Mantle (PM, McDonough and Sun, 1995) show spiked U-shaped patterns characterized by variable enrichments in the most incompatible elements relative to LREE (e.g., Th/La = 0.22–7.31 × PM), a strong enrichment in U and Pb relative to neighboring elements (U/Th ~ 28 × PM − Pb/Ce ~ 58 × PM), a systematic depletion in Nb, Ta, Zr and Hf relative to neighboring elements (e.g., Nb/La ~ 0.47 × PM; Zr/Sm ~ 0.25 × PM). Mantle wedge serpentinites are characterized by higher Zr/Hf (Zr/Hf = 0.95–1.27 × PM) compared to subducted serpentinites (Zr/Hf = 0.31–0.75 × PM).

The analyzed serpentinites display variable Sr anomalies (Fig. 2d, e); the absence of correlation between Eu_N/Eu^*_N (0.37–1.23) and Sr concentration pleads for Eu variation due to interaction with hydrothermal fluids during serpentinization and a only minimal effect of plagioclase (Paulick et al., 2006; Godard et al., 2009).

All studied samples are enriched in highly incompatible and fluid-mobile elements compared to PM values (e.g. As, Pb, U). These enrichments are attributed to extensive hydration with high fluid/rock ratios. Although substantial, the enrichments observed in the studied serpentinites are not as high as those observed in the Tso Morari mantle wedge serpentinites (Hattori and Guillot, 2003, 2007; Deschamps et al., 2010).

4.2. Lead isotopic compositions

Isotopic ratios for Pb for Cuban samples are reported in Table 3. $^{206}Pb/^{204}Pb$ varies from 17.88 to 19.02, $^{207}Pb/^{204}Pb$ from 15.58 to 15.67, and $^{208}Pb/^{204}Pb$ from 37.57 to 38.57. Samples are plotted in Fig. 3 and define a linear trend at the high $^{207}Pb/^{204}Pb$ edge of the field defined by Atlantic MORB along the Mid-Atlantic Ridge between 30°N and 30°S (compiled from PETDB, http://www.petdb.org) (Fig. 3a, c). Overall, serpentinite samples have more radiogenic $^{207}Pb/^{204}Pb$ compositions than Atlantic MORB and igneous rocks from Cuba (Blein et al., 2003; Marchesi et al., 2007; Fig. 3a, c) and define a trend parallel to, but much higher in $^{207}Pb/^{204}Pb$ than, the NHRL. Studied samples fall in an area typical of crustal materials such as data reported for the SW Amazon craton (Tohver et al., 2004) or data reported for sediments coming from the South American continent (Carpentier et al., 2008).

4.3. Mineral trace element compositions

Trace element compositions for serpentine phases, amphiboles, chlorites and iron oxides are reported in Table 4 (representative analyses) and Appendices 1 and 2.

4.3.1. Serpentine phases

Combining petrological and textural observations in the least altered samples and in situ analyses allows us to distinguish three types of serpentine related to the primary minerals from which they derive (olivine, orthopyroxene and clinopyroxene). Each serpentine type is characterized by its composition, in particular for REE and compatible trace elements, as illustrated in Figs. 4–6.

Serpentine minerals derived from olivine (serp-ol) are the most depleted in minor and trace elements (e.g., Sc: 2.7–12.3 μg/g, Ti: 5.2–114.8 μg/g, Yb < 0.068 μg/g, Y: 0.1–0.3 μg/g, Fig. 4). They are characterized by relatively flat C1-chondrite normalized REE patterns (Fig. 5a, b) although, in detail, we observe differences in REE fractionation between Dominican and Cuban samples: serp-ol from Cuba are LREE depleted with a strong variability in LREE/HREE ($0.08 < La_N/Yb_N < 2.77$; Figs. 4a, 5a) while most Dominican serp-ol are LREE enriched compared to MREE and HREE (La_N/Yb_N up to 8.15; Figs. 4a, 5b). Serp-ol REE patterns are similar to those of olivine separates in ultramafic nodules from southeastern British Columbia (Sun and Kerrich, 1995) and serpentinized olivine from Tso Morari serpentinites (Deschamps et al., 2010; Fig. 5c). These compositions are however enriched, especially in LREE, when compared to the olivines from the mantle wedge xenoliths sampled by the andesitic Avacha volcano (Kamchatka, Ionov, 2010; Fig. 5c).

Serpentine minerals after orthopyroxene (serp-opx; Figs. 4a and 5d, e) are characterized by higher REE (e.g. Yb ~ 0.03–0.24 μg/g; Fig. 4), Y (0.2–1.5 μg/g), Sc (5.8–49.3 μg/g) and Ti (38.1–468.6 μg/g) contents compared to serp-ol. Except for sample RD 94, a subducted serpentinite, serp-opx REE patterns are relatively flat ($Sm_N/Yb_N \sim 1.28$) with slight LREE enrichments (Fig. 5e), in particular in the Dominican Republic serpentinites ($La_N/Yb_N \sim 3.77$). These samples overlap in composition with the orthopyroxenes analyzed by Sun and Kerrich (1995) (Fig. 5f). Sample RD 94 is distinguished by its LREE depleted composition and plots in the field defined by serpentine after orthopyroxene from the Tso Morari serpentinite series (Deschamps et al., 2010). The REE heterogeneity of serp-opx is interpreted as evidence that the primary orthopyroxene REE content was (at least in part) preserved during serpentinization. Nevertheless, similar to serp-ol, the analyzed serp-opx compositions are enriched compared to the Avacha xenolith series (Ionov, 2010), suggesting a different mantle protolith.

Finally, serpentine formed after clinopyroxene (serp-cpx) presents strongly LREE depleted patterns (Fig. 5 g, h) with higher contents in moderately incompatible elements such as Sc, Y, Ti, Co, and V compared to serp-ol and serp-opx (Fig. 4). This group presents characteristics close to those of clinopyroxene analyzed in abyssal peridotites (Johnson et al., 1990; Dick and Natland, 1996; Hellebrand et al., 2002; Fig. 5i), suggesting a low mobility of REE, at least for HREE, and of moderately incompatible elements during serpentinization of primary phases (Andreani et al., 2009; Deschamps et al., 2010). It should be noted however that such depleted LREE patterns were not observed in the Tso Morari mantle wedge serpentinites (Deschamps et al., 2010). Serp-cpx patterns from Cuba display negative Eu anomaly ($0.40 < Eu_N/Eu^*_N < 0.85$), whereas the latter is not really marked in

Dominican serpentines derived from pyroxene (average of $Eu_N/Eu^*_N = 0.95$; Fig. 5 g, h).

On PM-normalized spidergrams (Fig. 6), nearly all serpentine patterns normalized to Primitive Mantle present enrichments in U, Pb and Cs (U/Th ~ 22.9 × PM; Pb/Ce ~ 37.6 × PM; Cs/Rb ~ 14.18 × PM). All Cuban serpentines (serp-ol, serp-opx and serp-cpx) are characterized by a higher content in Hf than Zr (0.08 × PM < Zr/Hf < 0.61 × PM, except two analyses at 1.11 × PM and 3.25 × PM). Both elements are depleted compared to neighboring elements (Zr/Sm ~ 0.33 × PM), whereas no particular behavior is discernable for these elements concerning Dominican serpentines (0.05 × PM < Zr/Hf < 19.35 × PM, average of 2.08 × PM; Zr/Sm ~ 1.73 × PM). A systematic depletion in Nb compared to Ta is observed in each types of serpentines for both locations (0.11 × PM < Nb/Ta < 0.91 × PM). Note that serpentine after orthopyroxene from

Table 4
Representative trace element analyses (LA–HR-ICP-MS) of serpentine minerals after olivine or pyroxene, amphiboles, chlorites and iron oxides from Cuban and Dominican serpentinites. All elements are in μg/g, except Si in wt.% (n.d. = not determined; b.d.l. = below detection limit). All analyses are reported in Appendixes 1 and 2.

Sample	CU 54	CU 54	CU 63	CU 63	CU 54	CU 63
	Abyssal	Abyssal	Wedge	Wedge	Abyssal	Wedge
	#1	#6	#10	#13	#17	#19
Spot size	77 μ	77 μ	122 μ	122 μ	77 μ	122 μ
Minerals	Serpentine	Serpentine	Serpentine	Serpentine	Serpentine	Serpentine
Group	1b	1b	3	3	1b	3
Primary mineral	Olivine	Olivine	Olivine	Olivine	Opx	Opx
All elements in %						
SiO_2	40.35	43.14	40.38	38.66	40.35	37.71
TiO_2	b.d.l.	b.d.l.	0.01	0.02	b.d.l.	0.01
Al_2O_3	1.28	1.16	0.39	0.27	1.28	0.09
Cr_2O_3	0.29	0.24	0.04	0.02	0.29	b.d.l.
MgO	37.34	32.80	35.49	33.78	37.34	37.29
FeO	6.51	5.92	4.37	2.77	6.51	2.39
MnO	0.11	0.06	0.07	3.52	0.11	0.06
NiO	0.07	0.10	0.78	1.48	0.07	0.30
CaO	0.01	b.d.l.	0.06	0.14	0.01	b.d.l.
Na_2O	0.02	0.01	0.02	0.01	0.02	b.d.l.
K_2O	b.d.l.	b.d.l.	0.01	0.02	b.d.l.	b.d.l.
Total	85.98	83.43	81.62	80.71	85.98	77.84
All elements in μg/g						
Li	0.68	3.67	0.37	0.46	1.76	0.23
B	6.6	15.7	94.8	39.5	16.2	27.5
Ca	188	279	636	317	169	223
Sc	2.7	8.6	7.8	4.3	8.7	49.3
Ti	31.7	69.3	17.4	6.5	86.9	208.9
V	14.9	47.7	10.6	6.9	47.6	142.6
Cr	2077	2722	173	109	4746	6225
Co	21.7	71.9	98.6	51.0	62.5	46.9
Ni	581	1708	11934	6653	1767	2430
Cu	2.3	16.7	3.7	1.0	9.8	0.8
Zn	15	58	36	13	44	14
As	0.74	1.66	0.31	0.23	2.37	0.18
Rb	0.053	0.270	0.094	b.d.l.	0.060	b.d.l.
Sr	0.372	1.583	5.050	1.701	1.392	1.127
Y	0.195	0.343	0.252	0.083	0.792	0.450
Zr	0.073	b.d.l.	0.140	0.050	0.166	0.172
Nb	0.010	0.035	n.d.	n.d.	0.026	0.004
Sb	0.04	0.07	0.03	0.02	0.09	0.07
Cs	0.032	0.027	n.d.	n.d.	0.009	b.d.l.
Ba	1.087	2.176	0.765	0.368	3.280	0.244
La	0.0226	0.0439	0.0124	0.0057	0.1004	0.0290
Ce	0.0468	0.0657	0.0106	b.d.l.	0.2510	0.0874
Pr	n.d.	0.0243	0.0016	0.0017	0.0401	0.0193
Nd	0.0453	0.1000	0.0337	b.d.l.	0.2380	0.0462
Sm	0.0397	0.0301	b.d.l.	b.d.l.	0.0951	0.0271
Eu	0.0062	b.d.l.	0.0112	n.d.	0.0249	b.d.l.
Gd	0.0283	0.0423	0.0245	0.0098	0.1000	0.0304
Tb	0.0051	0.0103	0.0071	n.d.	0.0172	0.0091
Dy	0.0326	0.0591	0.0249	0.0110	0.1481	0.0776
Ho	0.0072	0.0118	0.0101	0.0036	0.0348	0.0165
Er	0.0229	0.0423	0.0307	0.0098	0.1036	0.1035
Tm	0.0039	0.0038	0.0066	0.0032	0.0197	0.0119
Yb	0.0228	0.0586	0.0331	0.0200	0.1300	0.0776
Lu	0.0046	0.0103	0.0092	0.0058	0.0194	0.0216
Hf	0.0064	0.0114	0.0241	0.0100	0.0578	0.0159
Ta	n.d.	0.0025	b.d.l.	n.d.	n.d.	n.d.
Pb	0.050	0.125	0.034	0.016	0.348	0.009
Th	0.006	0.026	0.005	b.d.l.	0.026	0.002
U	0.007	0.027	0.004	0.001	0.339	0.009

Table 4 (*continued*)

Sample	CU 56	CU 65	RD 94	RD 34C	RD 36A	RD 94
	Abyssal	Abyssal	Abyssal	Wedge	Wedge	Abyssal
	#22	#31	#40	#44	#48	#54
Spot size	122 μ	122 μ	122 μ	122 μ	122 μ	122 μ
Minerals	Serpentine	Serpentine	Serpentine	Serpentine	Serpentine	Serpentine
Group	1a	1b	1a	3	3	1a
Primary mineral	Cpx	Cpx	Olivine	Olivine	Olivine	Opx gr.1
All elements in %						
SiO_2	42.01	41.98	40.82	43.54	42.77	41.22
TiO_2	0.05	b.d.l.	0.01	0.01	0.03	0.05
Al_2O_3	1.68	2.88	b.d.l.	0.02	0.06	1.38
Cr_2O_3	0.06	0.36	b.d.l.	b.d.l.	b.d.l.	0.14
MgO	39.46	33.20	36.64	36.37	39.19	34.24
FeO	3.14	8.08	6.24	4.59	3.64	7.05
MnO	0.07	0.13	0.02	0.05	0.00	0.12
NiO	0.07	0.25	0.36	0.41	0.24	0.10
CaO	0.03	0.04	0.02	0.04	0.02	0.03
Na_2O	0.02	b.d.l.	0.01	0.02	0.01	b.d.l.
K_2O	b.d.l.	b.d.l.	b.d.l.	b.d.l.	0.03	b.d.l.
Total	86.58	86.93	84.11	85.06	85.99	84.34
All elements in μg/g						
Li	0.43	0.79	0.63	0.25	0.53	3.20
B	48.0	8.1	17.2	23.2	33.5	32.2
Ca	326	163	76	206	149	330
Sc	20.5	14.3	12.3	4.2	3.8	15.9
Ti	351.6	69.3	114.8	11.3	14.4	277.9
V	70.6	173.4	82.8	8.2	3.4	46.5
Cr	2931	2879	3309	616	47	704
Co	77.4	102.5	61.8	74.3	181.1	42.6
Ni	b.d.l.	2244	2795	3079	b.d.l.	619
Cu	7.7	64.3	0.9	2.7	2.8	6.6
Zn	22	73	16	50	15	17
As	b.d.l.	0.83	0.13	0.27	0.13	0.13
Rb	0.409	0.107	0.576	0.073	n.d.	0.059
Sr	0.594	1.458	0.470	1.149	0.999	3.190
Y	1.306	3.090	0.145	0.200	0.255	0.200
Zr	0.441	0.283	0.083	0.110	0.225	0.387
Nb	0.005	0.087	0.005	0.014	0.071	0.006
Sb	b.d.l.	0.13	0.16	0.01	0.04	0.02
Cs	0.069	0.038	0.362	0.019	0.170	0.026
Ba	0.397	0.431	5.220	2.760	4.030	2.810
La	b.d.l.	0.0823	0.1028	0.0383	0.0803	0.0134
Ce	0.0103	0.3750	0.1115	0.0858	0.2287	0.0296
Pr	0.0061	0.0924	0.0133	0.0258	0.0719	0.0069
Nd	0.0749	0.5520	0.0775	0.0576	0.3020	0.0090
Sm	0.0552	0.2940	0.0152	0.0193	0.0528	b.d.l.
Eu	0.0221	0.0623	0.0067	0.0090	0.0269	0.0022
Gd	0.1186	0.3600	0.0286	0.0276	0.0735	0.0198
Tb	0.0266	0.0761	0.0022	0.0036	0.0115	0.0032
Dy	0.2070	0.5630	0.0246	0.0314	0.0587	0.0226
Ho	0.0453	0.1209	0.0052	0.0062	0.0155	0.0066
Er	0.1592	0.3830	0.0152	0.0157	0.0340	0.0380
Tm	0.0250	0.0631	0.0025	0.0038	0.0082	0.0085
Yb	0.1760	0.4270	0.0238	0.0291	0.0405	0.0790
Lu	0.0293	0.0752	0.0045	0.0072	0.0093	0.0187
Hf	0.0403	0.0168	0.0086	0.0030	0.1184	0.0144
Ta	n.d.	0.0100	n.d.	n.d.	0.0168	0.0013
Pb	0.039	0.090	0.073	0.354	0.627	0.183
Th	b.d.l.	0.041	0.007	0.023	0.197	0.014
U	0.006	0.003	0.015	0.041	0.057	0.005

(*continued on next page*)

Table 4 (*continued*)

Sample	RD 36A	RD 36A	RD 8E	RD 8E
	Wedge	Wedge	Abyssal	Abyssal
	#62	#64	#67	#69
Spot size	122 μ	122 μ	122 μ	122 μ
Minerals	Serpentine	Serpentine	Serpentine	Serpentine
Group	3	3	1b	1b
Primary mineral	Opx gr.2	Opx gr.2	Cpx	Cpx
All elements in %				
SiO_2	42.57	42.22	45.75	43.40
TiO_2	b.d.l.	b.d.l.	0.03	0.06
Al_2O_3	0.07	0.03	1.23	1.01
Cr_2O_3	0.05	b.d.l.	0.16	0.09
MgO	38.02	39.57	35.32	36.55
FeO	4.49	3.07	6.04	6.26
MnO	0.06	0.05	0.04	0.03
NiO	0.36	0.33	0.30	0.27
CaO	0.01	0.01	0.01	b.d.l.
Na_2O	b.d.l.	b.d.l.	b.d.l.	b.d.l.
K_2O	b.d.l.	b.d.l.	b.d.l.	0.02
Total	85.62	85.28	88.90	87.69
All elements in μg/g				
Li	1.29	0.43	0.47	2.04
B	80.8	27.8	19.8	16.7
Ca	424	2714	135	314
Sc	29.3	13.6	12.4	16.6
Ti	128.8	38.1	92.1	141.9
V	100.0	25.2	41.4	92.2
Cr	3197	b.d.l.	619	5338
Co	67.0	67.0	87.0	95.9
Ni	b.d.l.	b.d.l.	b.d.l.	b.d.l.
Cu	1.0	2.2	0.4	85.6
Zn	107	26	44	44
As	0.28	0.22	1.27	1.24
Rb	0.282	0.069	0.066	0.090
Sr	1.914	2.223	0.385	0.695
Y	0.624	0.775	0.934	1.237
Zr	0.742	0.503	1.159	2.820
Nb	0.223	0.184	0.021	0.017
Sb	0.04	0.09	0.14	0.20
Cs	0.186	0.022	0.025	0.040
Ba	8.170	3.890	0.117	0.133
La	0.1825	0.2229	0.0109	0.0441
Ce	0.7110	0.9880	0.0753	0.1637
Pr	0.0891	0.1641	0.0286	0.0416
Nd	0.4290	0.7000	0.1213	0.2410
Sm	0.1523	0.2340	0.0767	0.0889
Eu	0.0584	0.0546	0.0307	0.0378
Gd	0.1337	0.1690	0.1196	0.1780
Tb	0.0358	0.0340	0.0295	0.0364
Dy	0.1411	0.1950	0.1847	0.2403
Ho	0.0349	0.0330	0.0428	0.0598
Er	0.1067	0.1087	0.1153	0.1482
Tm	0.0259	0.0184	0.0219	0.0292
Yb	0.1888	0.1341	0.1293	0.1798
Lu	0.0326	0.0183	0.0284	0.0293
Hf	0.1106	0.0306	0.0374	0.0487
Ta	0.0478	0.0164	0.0043	0.0039
Pb	1.375	0.541	0.151	0.702
Th	0.578	0.104	0.009	0.054
U	0.228	0.066	0.123	0.043

(*continued on next page*)

Table 4 (*continued*)

Sample	CU 56	CU 62	CU 62	RD 36A	RD 62	RD 34C
	#76	#85	#86	#93	#105	#108
Spot size	122 μ	122 μ	122 μ	122 μ	122 μ	122 μ
Minerals	Iron oxide	Amphibole	Chlorite	Iron oxide	Amphibole	Chlorite
	Magnetite	Tremolite		Magnetite	Mg-Hbl	Bastite
Group	1a	2	2	3	2	3
All elements in %						
SiO_2	0.22	57.87	31.49	0.04	45.51	32.73
TiO_2	0.21	0.03	0.03	0.63	0.23	0.04
Al_2O_3	0.40	0.53	13.38	15.75	12.90	16.18
Cr_2O_3	9.82	0.04	0.15	37.87	0.08	1.80
MgO	0.63	22.68	28.80	6.61	15.48	31.06
FeO	79.81	4.57	6.11	34.64	7.43	2.78
MnO	0.47	0.13	0.04	0.42	0.07	0.02
NiO	0.06	0.10	0.19	0.22	0.04	0.21
CaO	0.04	11.41	0.04	b.d.l.	12.64	b.d.l.
Na_2O	b.d.l.	1.02	0.02	0.02	1.08	b.d.l.
K_2O	b.d.l.	0.09	b.d.l.	b.d.l.	0.70	b.d.l.
Total	91.67	98.48	80.26	96.20	96.16	84.82
All elements in μg/g						
Li	0.04	0.32	1.77	0.07	2.36	1.53
B	0.3	9.0	3.4	0.1	5.4	31.3
Ca	12	93104	5756	8	104089	7563
Sc	0.1	35.0	7.6	b.d.l.	43.7	20.8
Ti	89.2	168.2	65.5	16.5	1587.0	133.6
V	24.2	63.6	108.3	17.8	201.6	51.1
Cr	3830	321	2371	1743	427	2251
Co	23.7	43.9	84.7	4.0	49.8	87.3
Ni	b.d.l.	b.d.l.	b.d.l.	b.d.l.	b.d.l.	1266
Cu	211.8	0.2	1.5	0.1	0.6	2.4
Zn	118	29	58	33	8	49
As	b.d.l.	0.15	0.19	0.02	0.47	0.29
Rb	0.013	0.194	0.277	0.030	6.010	0.137
Sr	0.014	57.340	3.950	0.023	133.410	5.120
Y	0.007	12.880	0.492	0.001	6.370	0.595
Zr	0.008	1.402	0.700	0.119	8.620	30.140
Nb	0.003	0.051	0.078	0.004	0.306	0.119
Sb	b.d.l.	0.06	0.02	0.01	0.09	0.02
Cs	0.001	0.015	0.270	0.003	0.028	0.062
Ba	0.029	0.256	0.826	0.106	104.130	5.100
La	0.0060	0.0937	0.0901	0.0109	0.8630	0.4700
Ce	0.0748	1.1170	0.1479	0.0313	2.8340	1.4350
Pr	0.0098	0.2440	0.0230	0.0084	0.4610	0.1970
Nd	0.0027	1.8630	0.4210	0.0229	2.2890	0.8260
Sm	0.0010	1.0850	0.0637	0.0014	0.9000	0.1210
Eu	0.0026	0.2103	0.0313	0.0012	0.3000	0.0609
Gd	0.0026	1.8660	0.0803	0.0009	1.3010	0.1210
Tb	0.0007	0.3610	0.0290	0.0004	0.1969	0.0152
Dy	0.0019	2.7300	0.1064	0.0006	1.3480	0.1122
Ho	0.0003	0.5520	0.0304	0.0004	0.2587	0.0273
Er	0.0012	1.5250	0.0837	0.0003	0.6460	0.0772
Tm	0.0010	0.1988	0.0197	0.0003	0.0835	0.0114
Yb	0.0012	1.1800	0.0712	0.0004	0.4700	0.1680
Lu	0.0003	0.1506	0.0149	0.0002	0.0640	0.0282
Hf	0.0024	0.1558	0.0488	0.0025	0.3660	0.0118
Ta	0.0009	0.0167	0.0100	0.0003	0.0154	0.0079
Pb	0.029	0.980	0.181	0.017	0.964	0.386
Th	b.d.l.	0.255	0.047	0.008	0.071	0.145
U	0.027	0.046	0.367	0.003	0.045	0.082

Dominican Republic display two types of patterns as already observed with REE patterns: LREE-depleted patterns (sample RD 94) are also less enriched in all elements but remain U–Pb rich.

Some fluid-mobile elements, such as B (2–120 μg/g), As (0.1–2.4 μg/g), and Sb (0.01–0.6 μg/g) are moderately to highly enriched compared to Primitive Mantle values (from 2 up to 400 times PM values; McDonough and Sun, 1995) in all groups and for both locations (Fig. 7). Nevertheless, it appears in this context that antigorite from high-grade subducted samples (Group 1b) are slightly enriched in As, and, to a lesser extent, in Sb compared to the mixture of lizardite/chrysotile in low-grade subducted samples (Group 1a) and in mantle wedge serpentinites (Group 3). We note the particular case of Li (0.1–4.6 μg/g) which is on average depleted compared to PM values.

4.3.2. Amphiboles—pyroxenes

Amphiboles were analyzed in the two cumulates (Group 2; Fig. 8): CU 62 which is mainly composed of tremolite and RD 62 which is dominated by magnesio-hornblende. Trace elements are discriminating

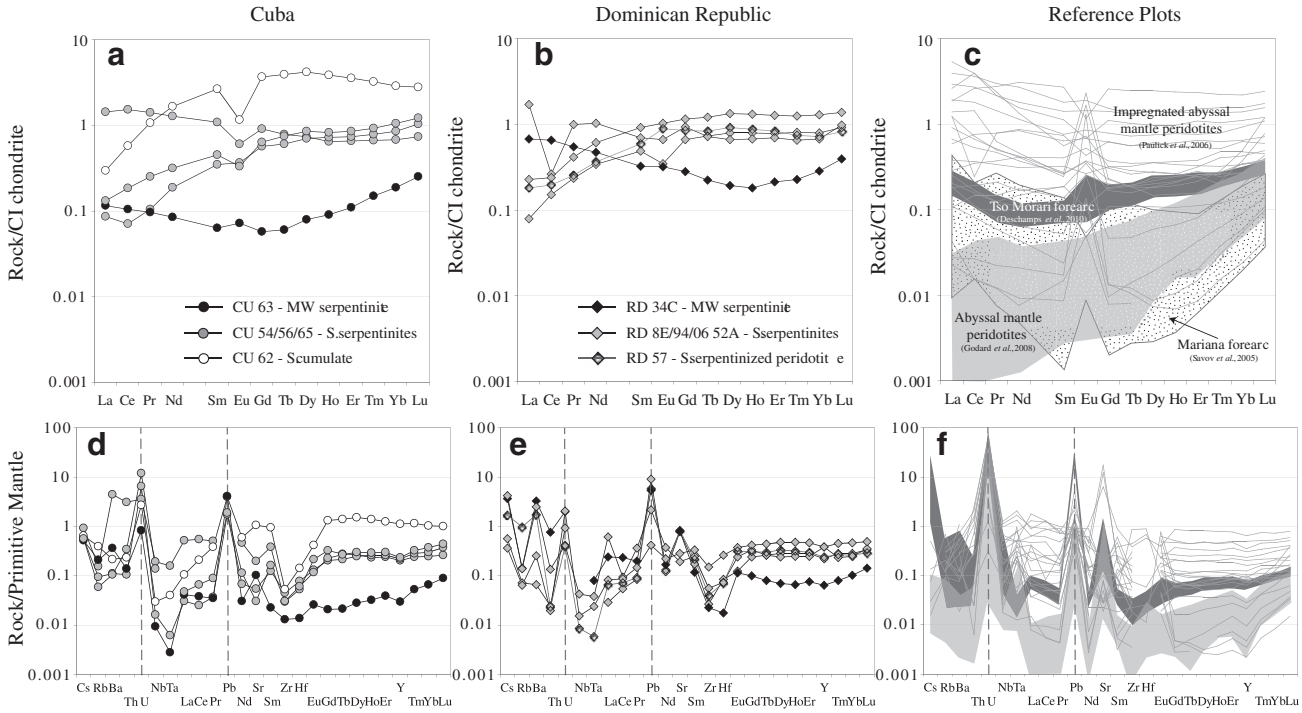

Fig. 2. a) and b) Chondrite-normalized bulk rock REE patterns for serpentinites from Cuba and Dominican Republic. d) and e) Primitive Mantle-normalized spidergrams. All samples are enriched in Cs, U and Pb, even sample RD 57, a serpentinized peridotites which preserves relics of primary minerals. Symbols in inset. Abbreviation: MW = Mantle wedge; S. = Subducted (oceanic lithosphere).c) and f) Reference plots. In both diagrams, patterns from abyssal mantle peridotites (gray field; Godard et al., 2008), impregnated abyssal mantle peridotites (gray patterns; Paulick et al., 2006), and serpentinites from hydrated mantle wedge (dark field: Tso Morari, Himalaya, Deschamps et al., 2010; dotted field: Mariana forearc, Savov et al., 2005) are shown for comparison. Chondrite and Primitive Mantle normalizing values were taken from McDonough and Sun (1995).

between the two groups: tremolites are LREE depleted ($0.065<La_N/Yb_N<0.134$) whereas Mg-hornblendes are HREE depleted ($1.4<La_N/Yb_N<4.8$; Fig. 8 a, b). Cumulate RD 62 in which the Mg-hornblendes were analyzed was sampled next to garnet peridotites, although the structural relationships between these rock types were difficult to establish in the field (Hattori et al., 2010). Nevertheless, the strong HREE depletion could point to a formation or re-equilibration of these amphiboles in the garnet stability field.

Tremolite are characterized by a strong Eu ($0.38<Eu_N/Eu^*_N<0.56$), Ba, Nb and Zr depletion, a slight enrichment in MREE, Pb, Th, Cs and strong enrichment in U. The bulk rock geochemistry of sample CU 62 (Fig. 2a) is similar and appears mainly inherited from tremolite (which represents ~60% of the sample volume). Mg-hornblendes from RD 62 are HFSE depleted and present relative enrichment in Rb, Ba, U, Pb and Sr. Their compositions plot in the depleted part of the field defined on the REE diagrams by amphiboles from ODP Site 920-MARK zone (Gillis and Meyer, 2001) and present similarities with amphiboles from talc-tremolite schists drilled in Atlantis Massif (Expedition IODP 304-305; Andreani, pers. com.).

Both amphiboles present enrichments in As (0.05–1.40 μg/g) and Sb (0.01–0.84 μg/g) close to those observed for serpentine phases. Li is enriched in amphibole (0.32–2.74 μg/g) compared to serpentine phase whereas B (3.93–9.33 μg/g) is less concentrated, but still higher than Primitive Mantle value. Magnesio-hornblende from sample RD 62 are enriched in Li (1.38–2.74 μg/g), B (5.3–9.3 μg/g), As (0.41–1.40 μg/g) and Sb (0.05–0.33 μg/g) compared to tremolite from sample CU 62 (Li, 0.32–1.52 μg/g; B, 3.9–9.2 μg/g; As, 0.05–0.15 μg/g; Sb, 0.01–0.07 μg/g, one analysis at 0.84 μg/g).

Two analyses of orthopyroxene with enstatite composition are also reported (Fig. 8 a, b). They present U-shape REE patterns but remain relatively close to the chondritic values, with slight enrichments in Ba, Th and U. Note the convergent characteristics between these orthopyroxenes and serpentine minerals derived from primary orthopyroxenes (Figs. 4c, d and 5d, e). Unfortunately, it was not possible during this study to analyze systematically the associated primary phases in serpentinite samples due to the strong alteration experienced by our samples and the size of relict phases, too small compared to the spot size.

4.3.3. Chlorites

Chlorites (clinochlore) were also analyzed in two samples (cumulate CU 62 and serpentine RD 34C). REE patterns are relatively homogeneous in term of MREE and HREE (from Sm to Lu), but differ strongly for LREE: $0.08<La_N/Sm_N<0.9$ for sample CU 62 and $2.4<La_N/Sm_N<4.8$ for sample RD 34C. Both extended patterns are dominated by Cs, Th, U, and Pb positive anomalies. Chlorite is enriched in As (0.07–0.73 μg/g), Sb (0.02–0.06 μg/g), and B (2.5–31.26 μg/g) compared to Primitive Mantle values (McDonough and Sun, 1995).

4.3.4. Iron oxides

Iron oxides (magnetites) are characterized by very low REE concentrations and for most elements, but show relative enrichments in U and Pb (from 0.1 PM to PM values). Concentrations in FME for iron oxides are lower than observed values for serpentine phases. The concentrations of B (0.007–0.43 μg/g), Li (up to 1.12 μg/g), U, Pb, Cs, and Ba are lower than the PM values, while As (up to 0.22 μg/g) and Sb (up to 0.084 μg/g) range from 0.1 to 10 times PM; note that one analysis (#89; Appendix 2) shows a concentration in As of 7.69 μg/g which might be due to a mixed analysis between an iron oxide and an arsenide grain similar to that observed by Hattori et al. (2005).

5. Discussion

The Cuban and Dominican serpentinites can be divided in two types. The first type (Group 1a and 1b) comprises the less depleted serpentinites; it is characterized by high bulk rock Al/Si ratio and low to moderate Cr# in chromite (Table 1) and it overlaps in composition

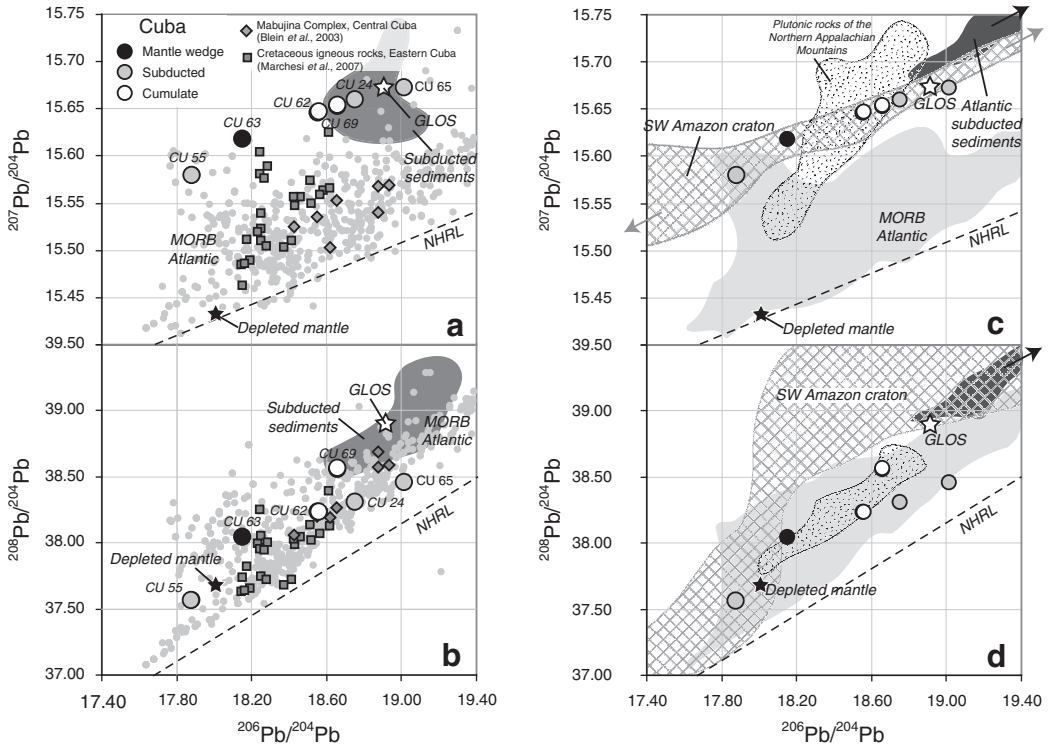

Fig. 3. $^{207}Pb/^{204}Pb$ (a) and $^{208}Pb/^{204}Pb$ (b) vs. $^{206}Pb/^{204}Pb$ diagrams for Cuban serpentinites (no age correction due to the open system; 2σ errors are smaller than the size point). Solid circle is for sample representing hydrated mantle wedge (CU 63), gray circles are for subducted serpentinites (CU 24, 55, 65), and open circles represent subducted hydrated cumulative rocks (CU 62, 69). Note that sample CU 55 is lizardite-bearing serpentinites (Group 1a; see text for definition) whereas samples CU 24 and CU 65 are antigorite-bearing serpentinites (Group 1b); CU 62 and CU 69 are hydrated cumulative rocks (Group 2) and CU 63 is lizardite-bearing serpentinite from mantle wedge (Group 3; see text for discussion). Isotopic field for Atlantic MORB along the mid-Atlantic ridge between 30°N and 30°S (little gray circles; compiled from PETDB, http://www.petdb.org/science.jsp) and Northern Hemisphere Reference Line (Hart, 1984) are reported for comparison. Average composition of global subducting sediments (GLOSS; Plank and Langmuir, 1998) is shown with a white star, whereas average composition of depleted mantle (Rehkämper and Hofmann, 1997) is shown with a black star. Isotopic compositions of cretaceous arc rocks coming from the Mabujina Complex in Central Cuba (gray squares; Blein et al., 2003) and cretaceous igneous rocks from the Eastern part of Cuba (gray diamonds; Marchesi et al., 2007) are shown for comparison.In figure c ($^{20}Pb/^{204}Pb$ vs. $^{206}Pb/^{204}Pb$) and d ($^{208}Pb/^{204}Pb$ vs. $^{206}Pb/^{204}Pb$), different isotopic fields are reported: plutonic rocks from the Northern Appalachian Mountains (North America; dotted area; Ayuso and Bevier, 1991), fields for SW Amazon craton are from Tohver et al. (2004), and isotopic field (dark gray) for sediments close to the trench of Lesser Antilles Arc (Carpentier et al., 2008). See text for explanations.

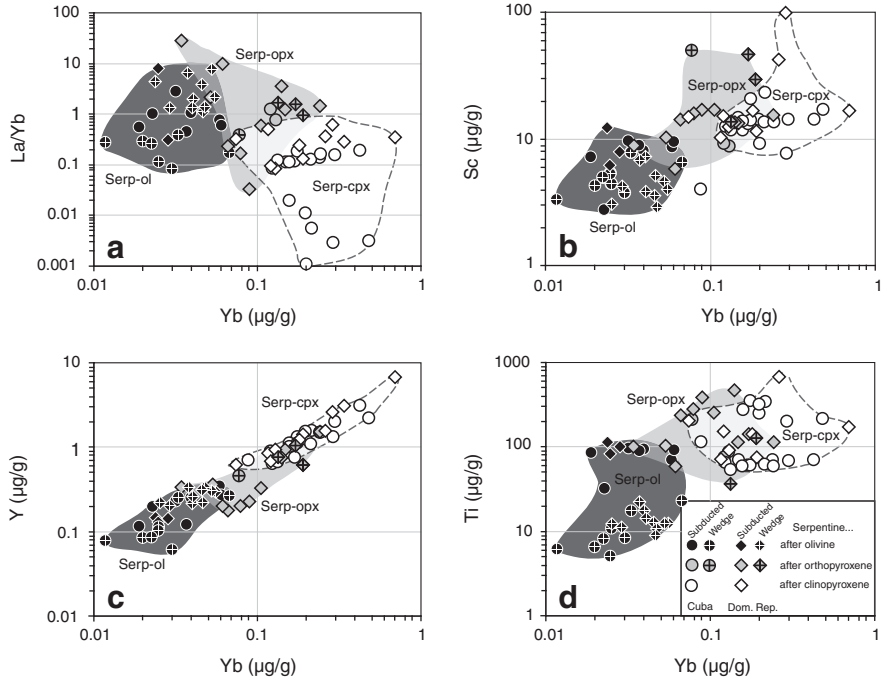

Fig. 4. Plots of La/Yb ratios and immobile trace elements (Sc, Y, and Ti) against Yb for serpentine phases. As shown by Deschamps et al. (2010), compatible elements and HREE allow distinguishing primary minerals. Three groups are recognized: serpentine after olivine (serp-ol; solid points and black field), serpentine after orthopyroxene (serp-opx; dark gray points and field) and serpentine after clinopyroxene (serp-cpx; open points and light gray field). Circles are Cuban samples and diamonds are Dominican samples. Samples coming from the mantle wedge (noted wedge in inset) are distinguished from samples from the subducted slab (noted subducted in inset) by a cross inside the symbol.

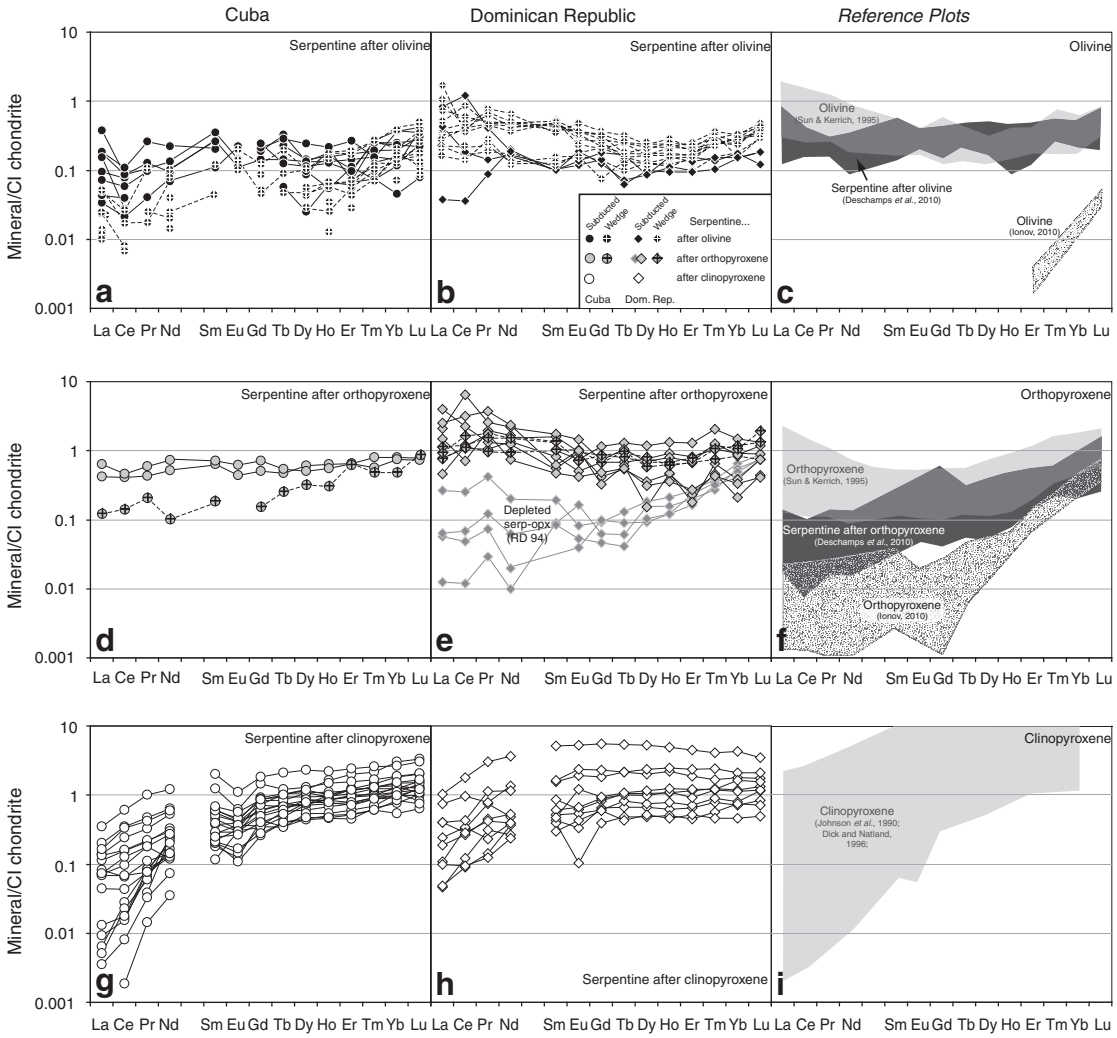

Fig. 5. Chondrite-normalized REE compositions of serpentines after olivine (a, b; black dot), after orthopyroxene (d, e; gray dot), and after clinopyroxene (g, h; open dot) in the serpentinites from Cuba and Dominican Republic (this study), compared to date from literature (c, f, i). Note the LREE-depleted composition of serpentine after orthopyroxene in sample RD 94. Symbols (in inset) for the Cuba and the Dominican Republic samples are the same as in Fig. 4. In Fig. 5c, light gray field represent olivine separates of ultramafic nodules from southeastern British Columbia, Canada (Sun and Kerrich, 1995), dotted field are for olivine from mantle wedge xenoliths from the andesitic Avacha volcano (Kamchatka; Ionov, 2010), and dark gray field represent serpentinized olivine from hydrated mantle wedge serpentinites in Tso Morari, Himalaya (Deschamps et al., 2010). In Fig. 5f, light gray (orthopyroxene) and dark gray (serpentinized orthopyroxene) fields are from Sun and Kerrich (1995) and Deschamps et al. (2010) respectively. Dotted field are for orthopyroxene from mantle wedge xenoliths from the andesitic Avacha volcano (Kamchatka; Ionov, 2010). In Fig. 5i, light gray field represent compiled values for clinopyroxene patterns from abyssal peridotites (Johnson et al., 1990; Dick and Natland, 1996; Hellebrand et al., 2002). Chondrite normalizing values for all diagrams were taken from McDonough and Sun (1995).

with abyssal peridotites as defined by Niu (2004) and with the variously altered impregnated abyssal peridotites sampled at the Mid-Atlantic Ridge (Paulick et al., 2006) (Fig. 2a, b, c). Together with the ultramafic cumulates (Group 2), they come from structural units interpreted as sampling the relics of the subducted Atlantic oceanic lithosphere. The second type of serpentinites (Group 3) has significantly more refractory compositions with low bulk rock Al/Si ratio (<0.03; Table 1), high Cr# in chromites (>0.50), a strong depletion in moderately incompatible elements (Y, Zr and HREE), and U-shaped REE patterns, similar to those of the mantle wedge serpentinites of Tso Morari (Deschamps et al., 2010; Fig. 2a, b, c). These serpentinites were sampled in structural units interpreted as sampling part of the hydrated mantle wedge of the extinct Greater Caribbean volcanic arc.

In situ analyses of serpentine phases revealed three types of REE patterns, which were correlated with different compositions of compatible minor and trace elements (e.g. Sc, Ti; Figs. 4, 5). Following Deschamps et al. (2010), these three groups are considered as representative of the primary mineralogy of the serpentinites: serpentine after olivine, orthopyroxene, or clinopyroxene. We note that samples having the most refractory bulk compositions, and interpreted as sampling the hydrated mantle wedge (Group 3) are dominated by serp-ol and serp-opx suggesting an initial mineralogy made of olivine and orthopyroxene. In addition, we never observed evidence of primary or altered clinopyroxenes in these samples. This observation is in agreement with the conclusion of Dick and Bullen (1984), Arai (1994) and Arai and Ishimaru (2008) about the refractory nature of peridotites from the mantle wedge due to high degrees of partial melting. In contrast, all subducted serpentinites are characterized by the occurrence of serpentinized pyroxenes (serp-opx and serp-cpx). Yet, in spite of these differences in modal compositions, the trace element composition of the serpentine minerals doesn't allow distinction of subducted from mantle wedge serpentinites. This suggests that although the geochemistry of the protolith is preserved, to some extent, at the scale of the bulk rock sample, chemical exchanges do occur during hydration but probably at a very local scale. For example, serpentinized olivine (serp-ol) display relatively homogeneous trace element patterns and compositions systematically more enriched than that of depleted olivine in subduction zone environments

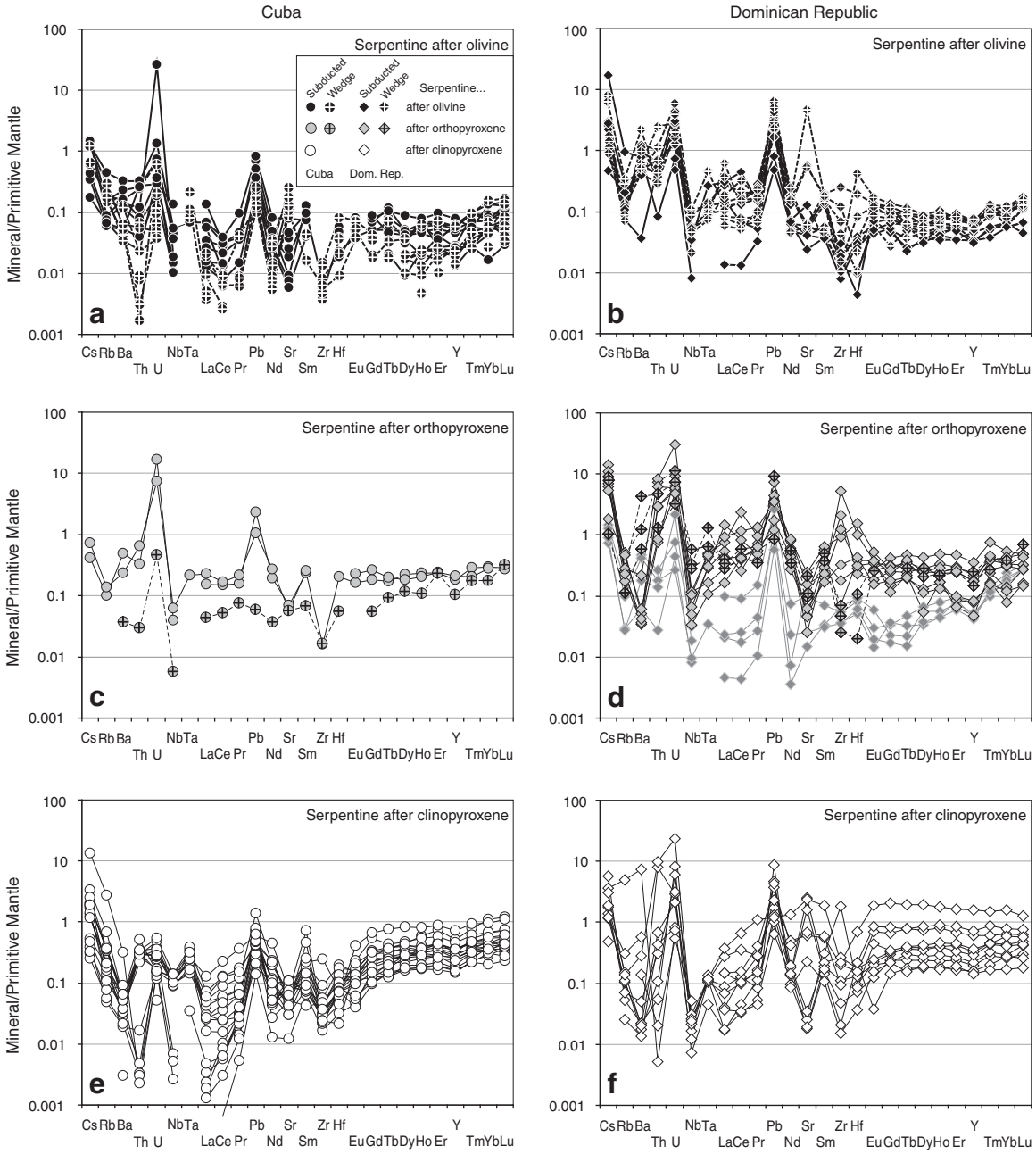

Fig. 6. Primitive Mantle normalized compositions of serpentine after olivine (a and b), serpentine after orthopyroxene (c and d), and serpentine after clinopyroxene (e and f). Symbols (in inset) for the Cuban and Dominican Republic samples are the same as in Figs. 4 and 5. In Fig. 6d, two groups of orthopyroxene are distinguished in Dominican serpentinites: LREE-enriched with black lines and LREE-depleted with gray lines (Sample RD 94).Normalizing values from McDonough and Sun (1995).

(Ionov, 2010; Fig. 5a, b,c), although they show good correlation with the metasomatised olivines analyzed by Sun and Kerrich (1995). Moreover, we note that the LREE content of many of the clinopyroxenes are actually lower than that of olivines. Despite the absence of primary olivine in our samples, we suggest that the LREE compositions of serp-ol could be explained by either a (L)REE-enrichment during serpentinization, or a redistribution and equilibration with the surrounding matrix composed of olivines and pyroxenes which imprint their (L)REE signature during serpentinization. This last option could explain the LREE enrichment of serp-ol to a level close to that of serp-(opx), which pleads in favor of localized homogenization processes.

While the major, minor and moderately incompatible trace element compositions of the analyzed serpentinites and serpentine minerals appear mostly dominated by the composition of their mantle and mineral protoliths, the (re-)distribution of fluid-mobile elements (FME) such as light elements (B, Li), semi volatile and chalcophile elements (As, Sb, Pb) and LILE (Sr, Rb, Cs, Ba and U) reflect the different conditions and settings during serpentinization. These elements being enriched in fluids interacting with the rock during alteration, they can be used to trace the sequence of serpentinization processes and the nature of percolating fluids, from the ridge to the subduction zone, during prograde metamorphism in the slab and the mantle wedge hydration.

5.1. Distribution of fluid-mobile elements in subducted serpentinites and associated cumulates

5.1.1. A ridge hydrothermal imprint on subducted serpentinites

In contrast to REE and to immobile highly incompatible elements, the FME compositions of serpentine phases in subducted serpentinites

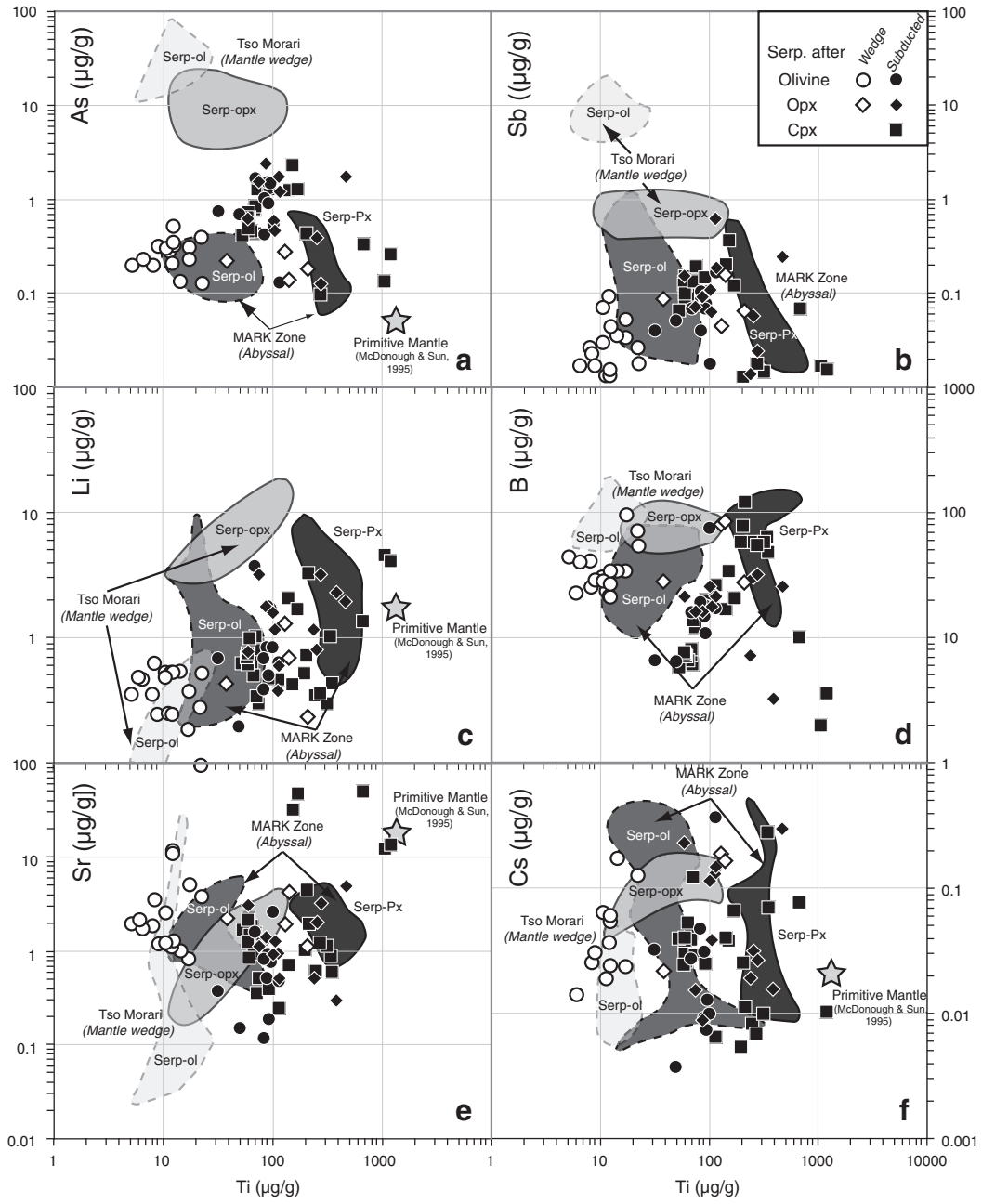

Fig. 7. Plots of As (a), Sb (b), Li (c), B (d), Sr (e), and Cs (f) versus Ti (µg/g) for serpentine minerals. Ti is discriminating between serpentine phases coming from mantle wedge serpentinites (low Ti, open symbols) and serpentinites sampling the subducted oceanic lithosphere (solid symbols), especially for serpentinized olivine. Compositions of serpentines from Tso Morari (hydrated mantle wedge, Deschamps et al., 2010) and from ODP Site 920-MARK Zone (Andreani et al., 2009) are also reported. Primitive Mantle values (gray stars) are from McDonough and Sun (1995).

(Group 1) do not depend on the nature of primary minerals (Figs. 7, 9). As, Sb, B and, to a lesser extent, Cs, Li, Pb and U are systematically enriched compared to Primitive Mantle values. Serpentine minerals plot in the field defined for serpentine minerals coming from ODP Site 920-MARK Zone (23°N MAR, Andreani et al., 2009) or from general subduction contexts (Kodolányi et al., 2012; Figs. 7, 9, 10), and present B-Li contents identical to those observed by Vils et al. (2008) in serpentine minerals from serpentinized peridotites from ODP Leg 209 (Holes 1272A and 1274A). On PM-normalized diagrams, As, Sb, B and, to a lesser extent, Cs, Li, Pb and U are enriched compared to all REE and to immobile highly incompatible elements; the distinct behavior of FME precludes a magmatic origin (late melt–rock interaction and refertilization) for the observed enrichments.

Except for As and Sb, serpentine minerals display the same patterns as fluids sampled at ultramafic hosted hydrothermal vents along slow spreading ridges (Logatchev, Rainbow, Snake Pit; Schmidt et al., 2007). Fluid/rock interactions, hydrothermal fluxes and serpentinization are controlled by seawater-derived fluids in these environments where mantle rocks are commonly exposed at the seafloor (Escartin and Cannat, 1999; Kuhn et al., 2004). We suggest that most of the observed FME variability and enrichments observed in the subducted serpentinites result from chemical exchanges related to hydrothermal circulations during serpentinization at the ridge, and maybe during the aging of the oceanic lithosphere (Mével, 2003). The higher concentrations in chalcophile elements (As, Sb) compared to hydrothermal fluids (Fig. 9) suggest that subducted serpentinites have undergone a secondary

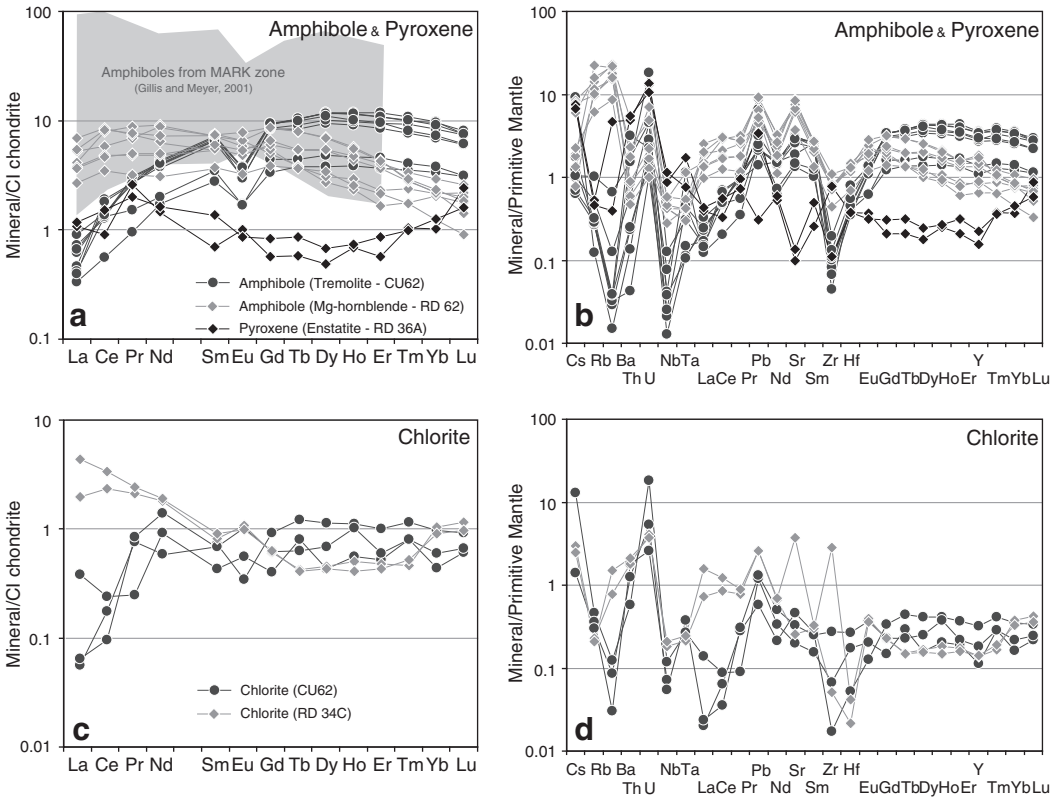

Fig. 8. a) Chondrite-normalized REE patterns and b) Primitive Mantle normalized compositions of primary pyroxenes (black diamonds) and amphiboles (black circles and gray diamonds) in cumulates form the subducted oceanic lithosphere. Gray field represent REE compositions of oceanic amphiboles in gabbros from ODP Site 920-MARK Zone (Gillis and Meyer, 2001).c) Chondrite-normalized REE patterns and d) Primitive Mantle normalized compositions of chlorite. See text for explanations.Normalizing values for all diagrams were taken from McDonough and Sun (1995).

addition of these elements, maybe during subduction; this point is discussed in Section 5.2.

The content of fluid-mobile elements is 10 to 100 times higher in the serpentine phases than in of seawater-derived hydrothermal fluids (Schmidt et al., 2007). This feature can be explained by high fluid/rock ratios (~20 up to 10^6) during serpentinization. The Sr isotope study of the Cuban samples indicated also that these samples had undergone high water/rock ratios during serpentinization (1 to 100; $0.70365 < {}^{87}Sr/{}^{86}Sr_{(120\ Ma)} < 0.70776$; Hattori and Guillot, 2007). These values are consistent with those typically obtained on abyssal serpentinites (e.g., Delacour et al., 2008), and suggest that serpentinites can be formed in a fluid dominated environment at ridges (Paulick et al., 2006).

No correlation exists between the estimated water content of the analyzed serpentine phases and their FME contents. We propose that, in spite of their complete hydration and the impossibility to incorporate more water, serpentinites are still infiltrated by fluids in chemical disequilibrium and the serpentine minerals continue to equilibrate with these fluids and to incorporate FME until equilibrium is reached. This hypothesis is in agreement with the relative homogeneity of FME compositions in serpentine phases from the different studied locations. In particular, we do not observe any significant difference between subducted (Groups 1a and b) and mantle wedge (Group 3) serpentinites, except for B, As and Sb (see Discussion sections 5.2 and 5.3). Furthermore, we note that FME enrichments appear to occur up to a threshold, probably due to the structure of serpentine minerals. This point is especially valid for boron compositions; we note a maximum uptake of B close to 100 μg/g, which is in agreement with those observed for oceanic serpentines (up to 139 μg/g B; Bonatti et al., 1984; Vils et al., 2008) and for forearc serpentines (up to 200 μg/g; Deschamps et al., 2010; Pabst et al., 2011; Kodolányi et al., 2012). Thus, due to this maximum storage capacity, boron is enriched by a factor of ~10 in serpentine compared to hydrothermal fluids, whereas As and Sb seem to reach higher values (~100 times).

5.1.2. Incorporation of fluid-mobile elements in serpentines

In spite of concentrations sometimes lower than PM values, U, Pb and, to a lesser extent, Cs are 10 to 100 times enriched in serpentine minerals, especially in those derived from primary pyroxenes, compared to hydrothermal fluids from oceanic environments (Fig. 9). This behavior is similar to that observed for Sb, As, and B, which are significantly enriched in serpentinites and associated serpentine phases compared to PM values (Fig. 9). In contrast, lithium presents, with a few exceptions (up to 2 times PM values), values systematically lower than those of PM for all groups of serpentine minerals (Fig. 10c) indicating a stronger loss in Li than in B and other FME. This behavior is similar to that observed by Vils et al. (2008) in serpentinized abyssal peridotites, where primary minerals (olivine and pyroxene) present higher Li concentrations than serpentine minerals. It is also consistent with the observation made on some hydrothermal fields where measured fluids are selectively enriched in Li, Sr and Rb but depleted in B compared to seawater (Schmidt et al., 2007).

Previous works on major elements have shown preferential loss of Ca during serpentinization (Miyashiro et al., 1969; Coleman and Keith, 1971; Komor et al., 1985; O'Hanley, 1996), favoring the formation of secondary carbonates. Sr has the same behavior as Ca and is preferentially concentrated in fluids. Lithium, which is characterized by a large ionic radius (0.76 Å) will be incorporated partly in the octahedral site and also in chrysotile core (Wunder et al., 2010), but seems to be mainly lost during serpentinization. The same conclusions can be made for Cs and Ba. On the basis of these observations, we suggest that the incorporation of fluid-mobile elements into serpentine

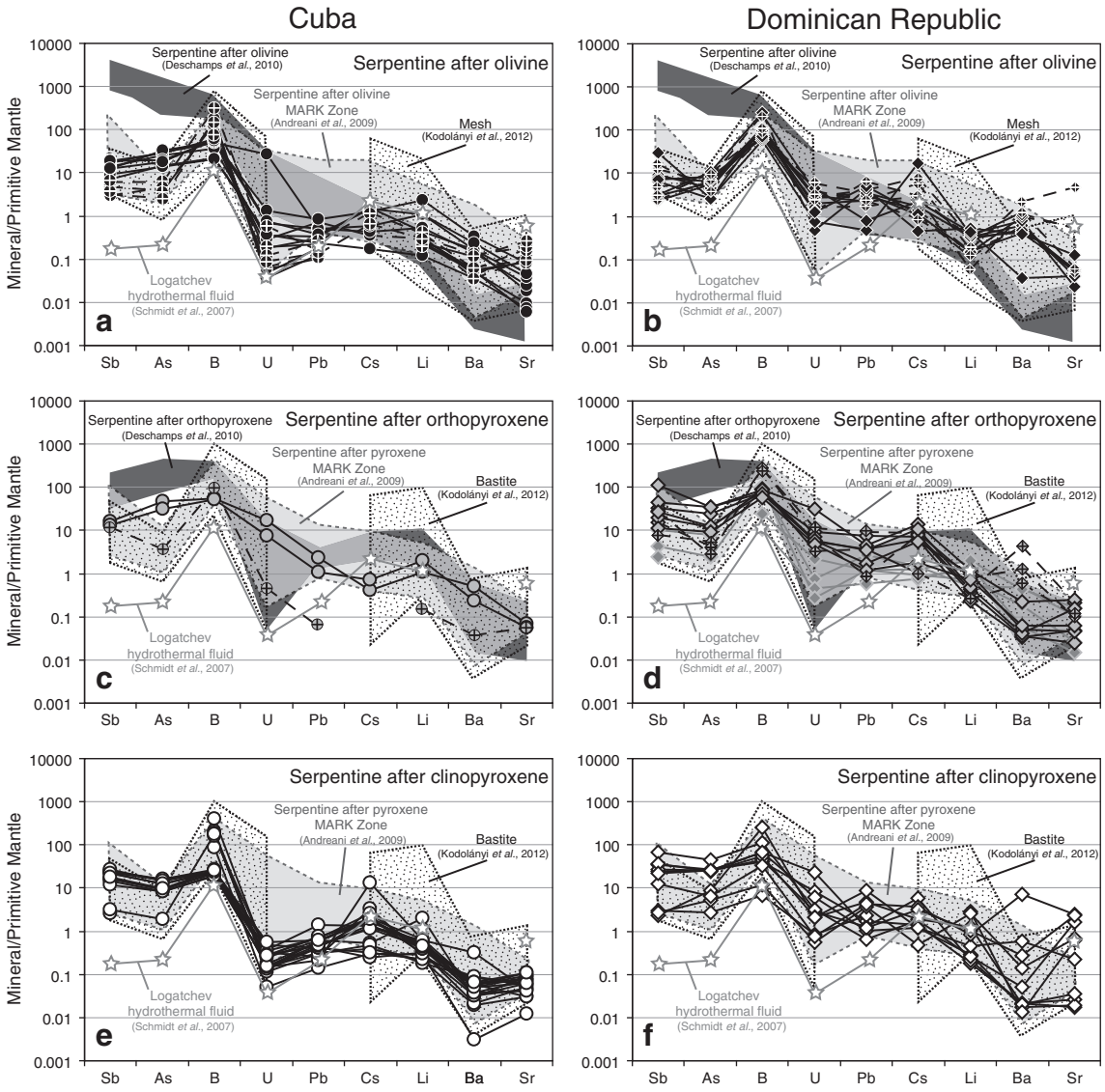

Fig. 9. Concentrations of fluid-mobile elements normalized to Primitive Mantle (McDonough and Sun, 1995) in serpentine derived from olivine (a, b; solid dots), orthopyroxene (c, d; gray dots), and clinopyroxene (e, f; open dots). Diagram modified from Hattori and Guillot (2003, 2007). The dark field (Fig. 9a–b) represents serpentinized olivine and the dark gray field (Fig. 9c–f) is for serpentinized orthopyroxene from Tso Morari serpentinites (Deschamps et al., 2010). The light gray field represents either serpentine after olivine (Fig. 9a–b) or serpentine after pyroxene (Fig. 9c–f) from ODP Site 920-MARK Zone (Andreani et al., 2009), whereas the dashed field represents either mesh (serpentine after olivine; Fig. 9a–b) or bastite (serpentine after pyroxene; Fig. 9c–f) from mid-ocean ridge, passive margin and forearc serpentinites (Kodolányi et al., 2012). The composition of hydrothermal fluids (Logatchev; Schmidt et al., 2007) is also reported for comparison (white stars; see text for discussion).

phases is controlled by their ionic potential defined by Railsback (2003) as the ratio charge/radius (i.e. z/r): elements with a low ionic potential ($z/r<2$, such as Li, Ca, Sr, Rb, Ba and Cs) are preferentially removed from the protolith and relatively enriched in percolating aqueous fluids during serpentinization, while elements with a high ionic potential ($z/r>2$; e.g. As, Sb, B, Pb) will be more easily incorporated into the crystal network.

5.1.3. Trapping of fluid-mobile elements in serpentinites during subduction-related metamorphism

Field evidence and the observed secondary mineral assemblage (chlorite, talc, tremolite) indicate that the subducted serpentinites have experienced blueschist to amphibolite metamorphism. Previous works on FME mobility during prograde metamorphism have demonstrated the mobility of some elements, such as As, Sb, B, Cs, during low grade metamorphism ($T<350\,°C$) associated with subduction for metasedimentary rocks (e.g. Bebout et al., 1999, 2007). Yet we observe the same range of concentrations of these elements in the studied subducted serpentines and in abyssal serpentines sampled near the mid-ocean ridge (Vils et al., 2008; Andreani et al., 2009) (Figs. 7, 9, 10). Considering that the FME enrichments found in abyssal serpentines sampled at the ridge are due to chemical exchanges during ridge hydrothermalism (Fig. 9), we interpret the similar compositions of abyssal and subducted serpentinites as evidence that once incorporated into serpentine phases, most of the FME stay immobile during subduction down to the lizardite/antigorite transition and probably up to 650–700 °C, temperature of the "antigorite breakdown" (Ulmer and Trommsdorff, 1995; Wunder and Schreyer, 1997; Wunder et al., 2001; Bromiley and Pawley, 2003). The lack of metamorphic olivine in the studied samples indicates that neither dehydration, nor partial dehydration occurred before the final "antigorite breakdown", in contrast to what is observed in the high-pressure serpentinites from the Betic Cordillera (Spain; Scambelluri et al., 2001a) or from the Alps (Scambelluri et al., 2001b).

Similar to Vils et al. (2011), Deschamps et al. (2011) and Kodolányi and Pettke (2011), we note a minor loss of boron during the transition chrysotile/lizardite to antigorite. However, the serpentinites sampled in Cuba and in the Dominican Republic show no evidence of a loss of

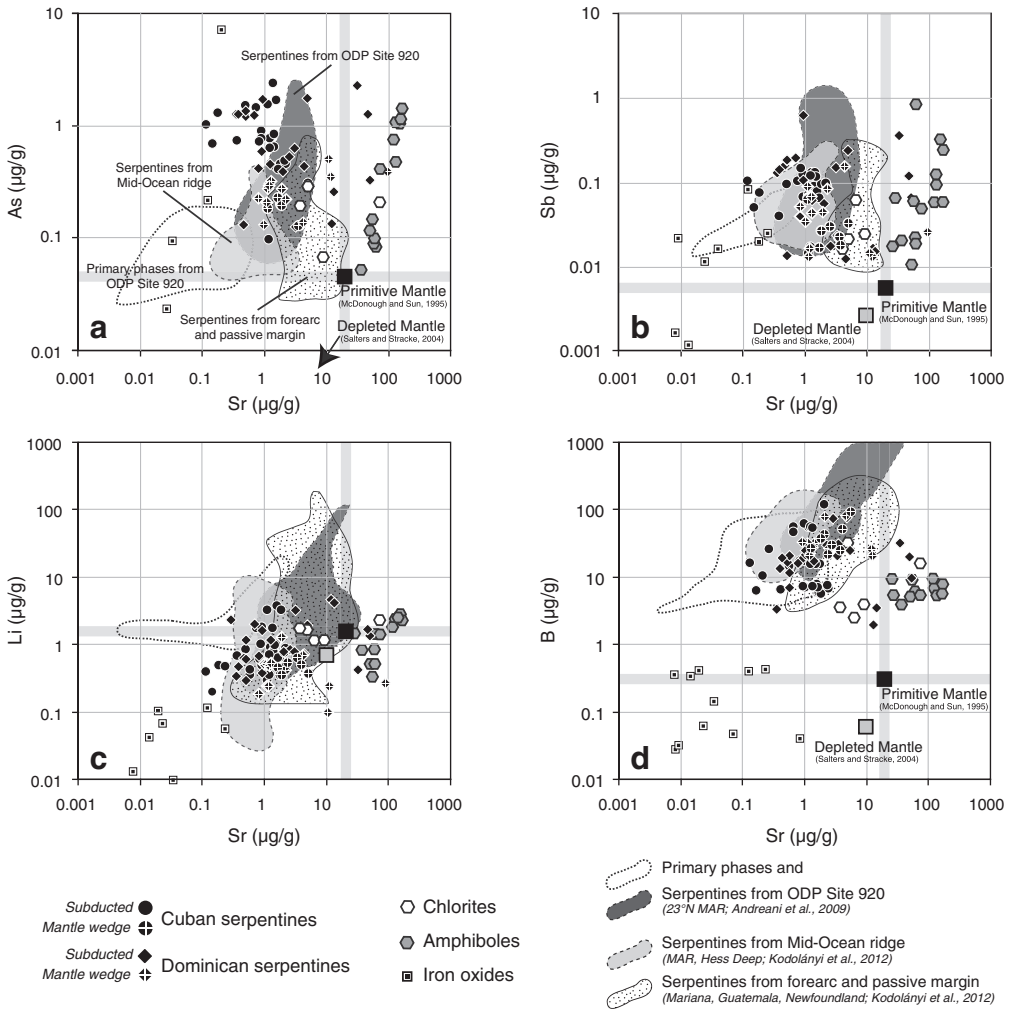

Fig. 10. Plots of As (a), Sb (b), Li (c), and B (d) versus Sr compositions (µg/g) for serpentine (solid circles and diamonds), chlorites (white hexagon), amphibole (gray hexagon) and iron oxides (black and white square) from Cuban and Dominican serpentinites. Serpentine from mantle wedge samples are marked with a cross inside the symbol. Compositions of serpentine (light gray field) and primary phases (white field) from ODP Site 920-MARK Zone (Andreani et al., 2009) and compositions of serpentine phases from mid-ocean ridge (Mid Atlantic ridge and Hess Deep; Dark gray field) and from passive margin (Iberia abyssal plain and Newfoundland) and forearc contexts (Mariana and Guatemala; Kodolányi et al., 2012) are also reported for comparison. Compositions of Primitive Mantle (black square) are after McDonough and Sun (1995) and depleted mantle (gray square) after Salters and Stracke (2004).

lithium or strontium in contrast to the serpentinites sampled in the Alps (Vils et al., 2011) and in Guatemala (Kodolányi and Pettke, 2011). Pelletier et al. (2008) showed that late stage metasomatism could develop during exhumation of high pressure terranes and induce secondary enrichments in fluid-mobile elements, but only over very short distances from the contact with metasediments (100–150 m). Similarly, a late FME-enrichment process could have affected the studied serpentinites and thus explain the relative enrichments in Li and Sr compared to those studied by Vils et al. (2011) and Kodolányi and Pettke (2011). However, our study was carried out mostly on serpentinites sampled at the center of large and well defined structural units, which led us to eliminate this hypothesis to explain these differences in the observed mobility of B and Li in subducted serpentinites. Alternatively, we propose that these differences may reflect the lithology and composition of the downwelling slabs (crust-dominated fast spread lithosphere vs. mantle-dominated slow spread lithosphere) and the water partial pressure during the lizardite/antigorite transition in these different subduction settings (e.g. Van Keken et al., 2011).

5.2. Evidence for a second stage of serpentinization during subduction

Hattori and Guillot (2007) have shown that the Sr isotopic signature of the studied Cuban serpentinites varies between upper mantle and contemporaneous marine Sr values ($0.70365 < {}^{87}Sr/{}^{86}Sr_{(120\ Ma)} < 0.70776$). The highest $^{87}Sr/^{86}Sr$ values are higher than Tertiary marine Sr values. Hattori and Guillot (2007) interpreted the occurrence of such radiogenic samples as evidence for a contribution from sediment-derived fluids in the formation of these serpentinites. Our lead isotope data and trace element data support, in part, this interpretation but reveal also a complex pattern of contamination by sediment-derived fluids.

5.2.1. Identification of subduction related-metasomatising fluids and geodynamic implications

Cuban serpentinites are characterized by radiogenic compositions, especially in $^{207}Pb/^{204}Pb$, typical of island arc environments (Table 3; Fig. 3a). Although the studied serpentinites derive from different protoliths and geological settings (peridotites and cumulates from the proto-Atlantic oceanic lithosphere and parts of the hydrated mantle wedge), all samples plot on a linear trend in $^{207}Pb/^{204}Pb$ versus $^{206}Pb/^{204}Pb$ space (Fig. 3a). We tested the possibility that this linear trend could derive from the post-emplacement decay of uranium series nuclides: the calculated age is 1.22 Ga, a value that is clearly not consistent with the Jurassic age of our samples.

When compared with arc volcanic rocks from Cuba (Blein et al., 2003; Marchesi et al., 2007), our samples plot on the same trend on

the $^{208}Pb/^{204}Pb$ versus $^{206}Pb/^{204}Pb$ diagram, but differ by their more radiogenic $^{207}Pb/^{204}Pb$ ratios (Fig. 3a). Mixing between a depleted mantle source and the GLOSS (Global subducting sediments, Plank and Langmuir, 1998) cannot explain the trend observed for Cuban serpentinites (Fig. 3c, d) and a high $^{207}Pb/^{204}Pb$ component is needed to account for the observed variations.

No preferential enrichment or particular behavior, depending on the initial protolith of serpentinites, is observed, as well as no particular trends and coupling between Pb- and Sr isotopes. We note that lizardite-bearing sample (Group 1a, CU 55) is less radiogenic that antigorite-bearing samples (Group 1b, CU 24 and CU 65) which could be explained by a stronger influence of a sedimentary-rich fluid for the latter.

The proto-Caribbean oceanic crust is inferred to have been formed in the Middle Jurassic/Early Cretaceous during the opening of a narrow oceanic basin between North and South America continents (Ross and Scotese, 1988; Morris et al., 1990; Pindell and Barrett, 1990; Sawyer et al., 1991; Meschede and Frisch, 1998; Mann, 1999). The composition of the sediments entering the subduction zone was influenced by the lithologies coming from both continents (Marchesi et al., 2007). Yet, mixing between mantle composition and an average of plutonic rocks from the Northern Appalachians Mountains representative of the North American craton (Ayuso and Bevier, 1991) or an average of sediments subducting at the level of the Lesser Antilles Arc (Carpentier et al., 2008) does not really explain the radiogenic composition of Cuban serpentinites (Fig. 3c, d).

In contrast, the studied serpentinites Pb-isotopic compositions overlap with those of the sediments from the South American continent. They are perfectly aligned along a trend defined by rocks coming from the SW Amazon craton (Tohver et al., 2004) and the field of sediments close to the trench of the Lesser Antilles Arc (Carpentier et al., 2008). For the latter, it was demonstrated that their compositions (high Pb isotopic ratios) are partially controlled by radiogenic detrital materials from the Brazilian and Guyana cratons (Carpentier et al., 2008). Acquisition of a detrital-rich Pb signature in a forearc context during formation of the Greater Carribean arc is consistent with the conclusions of Marchesi et al. (2007) on Cretaceous magmatic rocks from the Cuban paleo-island arc. We propose that the fluids that contaminated the Cuban serpentinites were enriched in Pb with high $^{207}Pb/^{204}Pb$ ratios and that these fluids originated from the dehydration of sediments deriving from the South American craton. This process appears to have erased totally the initial Pb isotopic signature of the mantle protolith, especially in $^{207}Pb/^{204}Pb$ versus $^{206}Pb/^{204}Pb$ space.

5.2.2. Arsenic and antimony: tracers of sedimentary influence

As and, to a lesser extent, Sb contents are enriched in antigorite from high-grade subducted serpentinites (Group 1b; As: 0.41–2.37 μg/g and Sb: 0.02–0.15 μg/g), compared to lizardite/chrysotile from the low-grade subducted serpentinites (Group 1a; As: 0.10–0.53 μg/g and Sb: 0.01–0.16 μg/g) and from the mantle wedge (Group 3; 0.13–0.31 and 0.02–0.07 μg/g respectively). These elements are also enriched compared to fluids sampled at ultramafic hosted hydrothermal vents at ridges (Logatchev, Rainbow, Snake Pit; Schmidt et al., 2007; Fig. 9).

The trends defined by Ba and Sr vs. B (Fig. 11) for both subducted and mantle wedge serpentines suggest that these elements are equally enriched in hydrating fluids. Such enrichment could be acquired during

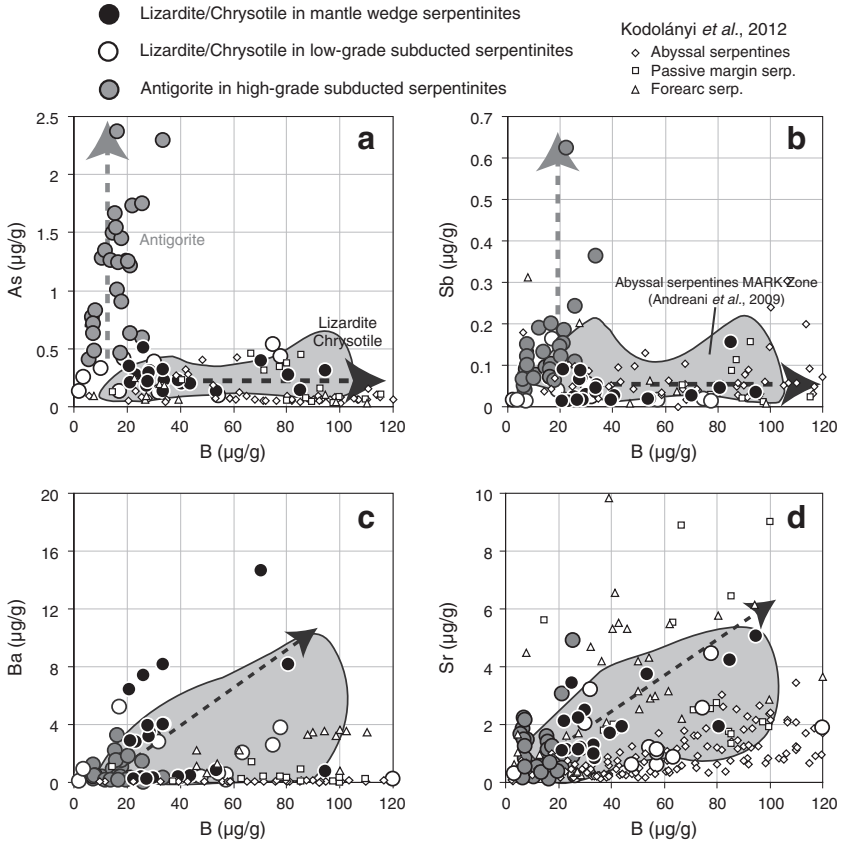

Fig. 11. Compositions of As (a), Sb (b), Ba (c), and Sr (d) versus B (μg/g) for serpentine minerals from subducted serpentinites (low-grade samples with lizardite/chrysotile: white circles; high-grade samples with antigorite: gray circles) and from mantle wedge serpentinites (solid circles). Serpentine compositions from abyssal (white diamond), passive margin (white square) and forearc (white triangle) contexts are reported for comparison (Kodolányi et al., 2012). Gray field are for serpentine minerals (mostly lizardite) from abyssal serpentinites (ODP Site 920-MARK Zone; Andreani et al., 2009). Dashed lines with arrows represent the chemical evolution of serpentine phases during hydration and associated FME enrichment. We observe clearly different distributions of As, Sb and B in subducted and mantle wedge serpentinites. Such observations indicate different fluid compositions at the origin of these serpentines (see text for explanations; errors are lower than the size point).

seawater interactions, as indicated by the observed compositions close to those observed in subduction-related serpentinites (Kodolányi et al., 2012) or in abyssal serpentinites from ODP Site 920-MARK (Andreani et al., 2009). But two different trends are observed in As vs. B and Sb vs. B diagrams. Fluids which percolate through subducted antigorite-bearing-serpentinites (Group 1b) are greatly enriched in As and Sb compared to the fluids at the origin of low-grade subducted serpentinites (Group 1a) and those percolating later mantle wedge (Group 3).

As discussed in the previous section, subducted serpentinites (Group 1) acquired during subduction a lead isotopic composition typical of island arc magmas that is particularly well marked for $^{206}Pb/^{204}Pb$ and $^{208}Pb/^{204}Pb$ in antigorite-bearing serpentinites (Group 1b) which were subducted to greater depth. This signature suggests a secondary imprint from sediment-derived fluids. Sediments are characterized by high As and Sb concentrations (Plank and Ludden, 1992; Leeman et al., 1994; Jochum and Verma, 1996; Leeman and Sisson, 1996). The high As and Sb contents measured in antigorite-bearing serpentinites could result from a second stage of serpentinization associated with the circulation of the same sediment-derived Pb-radiogenic fluids.

The As and Sb over-enrichment in antigorite-bearing samples (Group 1b) suggests that sediment-derived fluids (As-, Sb-rich, and radiogenic) percolated through serpentinites at temperatures ranging from 250 to 400 °C corresponding to the lizardite–antigorite transition. Although limited, our data on cumulates are consistent with this scenario. The magnesio-hornblende-bearing cumulate (RD 34C) is likely to have experienced higher P–T conditions than the tremolite-bearing cumulate (CU 62); it is also enriched in As and Sb (but also in B and Li) compared to sample CU 62. It probably interacted with the same As–Sb rich sedimentary-derived fluids during subduction.

5.2.3. How and where is the sedimentary signature acquired?

Different geodynamic scenarios could explain the sedimentary signature observed in the subducted serpentinites (over-enrichment in As and Sb, radiogenic compositions in Pb-isotopes).

First, fluids derived from sedimentary deposits close to the ridge could infiltrate the serpentinized mantle lithosphere during aging of the oceanic lithosphere. This model is compatible with the paleogeographic reconstitution of basin opening at that time (Pindell et al., 2005). Occurrence of sediments close to the ridge could have modified the hydrothermal signature and then the isotopic composition of abyssal peridotites. But the over-enrichment in As and Sb seems to occur at the lizardite/antigorite transition, that is at increasing P–T conditions, which is not characteristic of ridge environments and suggests that this sedimentary signature is acquired in a subduction context.

Second, aqueous fluids released by dehydration of the downwelling altered oceanic mantle, crust and sediments percolate upward through the downwelling slab and the mantle wedge. Rüpke et al. (2004) estimate that half of the 7% of water of GLOSS sediments (Plank and Langmuir, 1998) is released in the first 50 km of subduction. However, this simple model is not consistent with our observations, which indicate that the serpentinites, i.e. the lowermost part of the slab, are contaminated by sediment-derived fluids.

Third, fluids produced in the accretionary prism infiltrate through the bending faults (Fig. 12) formed at the outer rise/trench into the crust and upper mantle of subducting slabs (Savage, 1969; Kirby et al., 1996; Jiao et al., 2000; Peacock, 2001; Ranero et al., 2003, 2005). But, the highest As content is related to antigorite formation at high temperatures: this suggests that contamination by sediment-derived fluids was most efficient at temperatures of about 300 to 400 °C corresponding to the lizardite/antigorite transition.

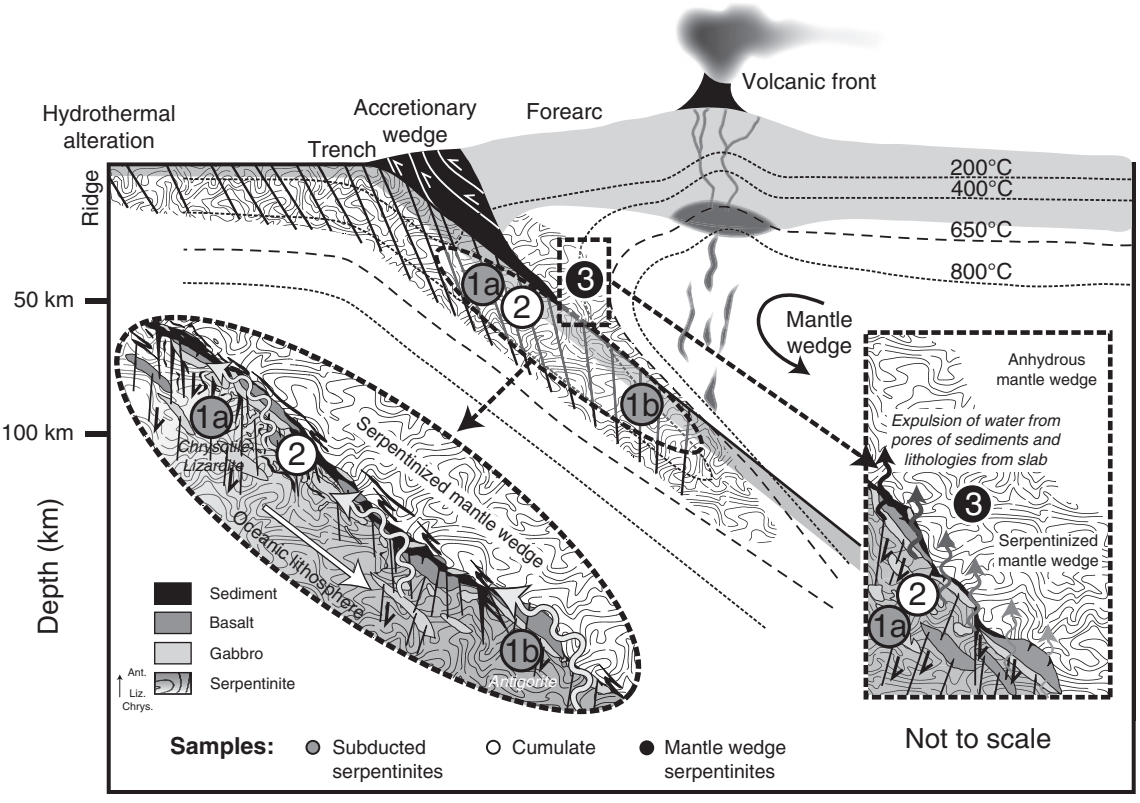

Fig. 12. Schematic sketch illustrating the geological context during subduction-related serpentinization of the studied samples before their exhumation. Gray point marked with 1a is for low-grade (lizardite/chrysotile) subducted serpentinites which record mainly hydrothermal serpentinization at the ridge in a slow spreading context. Gray circle marked with 1b is for high-grade subducted serpentinites (antigorite) representing also subducted abyssal serpentinites but which have undergone higher P–T conditions; they experienced a secondary serpentinization while in the subduction channel, with a strong influence of sediment-derived fluids, probably during the lizardite/antigorite transition, and marked by an over-enrichment in As–Sb. White circle marked 2 represent subducted cumulates. Solid circle marked 3 is for serpentinites (lizardite/chrysotile) deriving from the hydration of the mantle wedge by pore-fluids released from lithologies constitutive of the slab; influence of sediments is very limited. See text for more details.

Fourth, contamination by sediment-derived fluids occurred at depth within the subduction channel where sediments and serpentinites are mechanically mixed and could exchange their geochemical characteristics. Bebout et al. (1999) showed that As and Sb are released from metasediments between 350 and 400 °C at 0.9–1.2 GPa (lawsonite–blueschists to epidote–blueschists transition) during prograde metamorphism. As- and Sb-rich fluids resulting from the dehydration of metasediments are good candidates for the As and Sb over-enrichments observed in high-grade serpentinites. Field observations provide no evidence for or against this scenario: serpentinites from Group 1b outcrop either as (i) serpentinites constituting a matrix hosting mafic + sedimentary rocks like in a channel (Dominican Republic, samples RD 8E and RD06 52A), or as (ii) lenses of serpentinite in a metamorphized sedimentary matrix (Cuba, sample CU 65).

We favor this last scenario for the formation of the Cuban and Dominican serpentinites as it best fits our observations (Fig. 12): pore water and FME, especially As and Sb (Bebout et al., 1999), are expelled from downgoing subducted hydrated sediments and migrate upward and laterally (Bebout and Barton, 1989) in the subduction channel beneath the forearc domain (Guillot et al., 2009 and references therein) which is controlled by mechanical and metasomatic mixing processes.

5.3. Geochemical differences between mantle wedge and subducted serpentines: source and nature of hydrating fluid

As indicated previously, mantle wedge serpentinites are characterized by refractory compositions and strong depletion in moderately incompatible elements. Nevertheless, these samples are also enriched in FME due to serpentinization processes. Undoubtedly, these samples have experienced a complex history within the mantle wedge and the following scenario is proposed.

First, mantle wedge peridotites experienced partial melting triggered by the infiltration of slab-derived fluids which produced their highly refractory and Ti depleted compositions typical of peridotites sampled in subduction zone environments (e.g. Arai and Ishimaru, 2008). The analyzed serpentines have low Ti content similar to those observed in serpentines after olivine from Tso Morari serpentinites (Deschamps et al., 2010; Fig. 7). The same Ti-depletion characterizes also secondary hydrous phases, such as phlogopite and pargasite, in mantle wedge xenoliths (Arai and Ishimaru, 2008). The analyses of primary orthopyroxene (enstatite—RD 36A) and secondary chlorite (RD 34C) from mantle wedge serpentinites are characterized by U-shaped REE patterns with slight enrichment in LREE (Fig. 7a, c). Fluids released from the subducting slab into the mantle wedge are hotter ($T \approx 300$ °C) than the fluids at the origin of subducted samples, and consequently slightly enriched in LREEs (Gammons et al., 1996) relative to HFSE which remains insoluble (Keppler, 1996). Such fluids could be responsible for the LREE enrichment in chlorite and low Ti contents observed in serpentine phases.

Second, the refractory mantle wedge peridotites are serpentinized. Due to the mantle wedge dynamics, we propose that the refractory peridotites are (1) exhumed or protruded in an upwelling movement (e.g. Saumur et al., 2010), or (2) mechanically incorporated to the subduction channel, but are still infiltrated by slab-derived fluids. At low temperature (<350 °C) these fluids trigger serpentinization. Thus, serpentine phases (lizardite and chrysotile essentially) in mantle wedge samples (Group 3) present relatively the same range of compositions for mostly of the FME compared to the low-grade (Group 1a) and high-grade (Group 1b) subducted serpentines. However FME do not allow discriminating between the source of contaminating fluids: seawater, hydrothermal fluids or aqueous fluids released from a subducting slab, because all of them are theoretically enriched in these elements (e.g. Pearce, 1983; Tatsumi, 1986; Brenan et al., 1995; Keppler, 1996; Kogiso et al., 1997; Stalder et al., 1998; Li and Lee, 2006; Schmidt et al., 2007). Note that the sedimentary signature of mantle wedge sample CU 63 is consistent with the models of sediment dehydration into subduction zones, but this sedimentary signature is less important than that observed in antigorite-bearing serpentinites from Group 1b (Fig. 3). This suggests that contamination by sediment-derived fluids was probably minor in mantle wedge samples. Another possible scenario would be that the fluid percolates the mantle wedge as focussed fluid flow rather than pervasive fluid flow and that our sampling is not sufficient to catch the dehydration veins having a more radiogenic signature.

We note an interesting feature with B compositions (Figs. 10, 11): it appears that mantle wedge serpentines are enriched in B compared to antigorite-bearing samples and present the same enrichment as observed in lizardite-bearing subducted serpentinites. Bebout et al. (1999) have shown that B is removed from metasedimentary rocks around 200–300 °C at 0.6–0.8 GPa (lawsonite–albite to lawsonite–blueschists transition) and before As and Sb. We propose that these fluids were liberated from the slab at a depth comprised between the isotherm where dehydration of sediments occurs ($T < 300$ °C, depth < 50 km; Rüpke et al., 2004) and the isotherms marking the beginning of the stability of antigorite into the mantle wedge (isotherm > 250–400 °C; Berman et al., 1986).

6. Conclusions

Using bulk-rock and in situ trace element analyses coupled with Pb isotopic systematics, we distinguished three stages of serpentinization in the series of serpentinites sampled in the Cuban and Dominican Republic, each stage characterized by fluids of different origins and FME content.

(1) Subducted serpentinites derive from a fertile mantle protolith and are associated in the field with altered ultramafic cumulates mainly composed of amphibole and chlorite. These samples are considered as relics of the subducted then exhumed slabs. In situ analyses of these serpentinites display three types of serpentines in term of REE and compatible elements reflecting primary olivine, clinopyroxene or orthopyroxene. Serpentine minerals (lizardite, chrysotile and antigorite) and hydrated phases in associated cumulate are characterized by strong enrichments in fluid-mobile elements (B, As, Sb, Li, Cs, U, Pb) close to those observed in serpentinites in abyssal environments. The subducted serpentinites are interpreted as being formed at the ridge or during aging of a mantle-dominated oceanic lithosphere by interaction with seawater-derived hydrothermal fluids. The similarity of the FME enrichment (with the exception of As and Sb for antigorite) observed in the serpentine phases from abyssal serpentinites and from samples coming from the subducted slab suggest that FME stay trapped in these serpentine phases during subduction. Our data suggest that this is true, down to the depth of the "antigorite breakdown" (650–700 °C) (not observed in our sampling). Except for B, no evidence of mobility of FME is observed despite prograde metamorphism.

(2) Subducted serpentinites are divided in two groups: lizardite-bearing samples and antigorite-bearing samples. High-grade serpentinites are distinguished by enriched As and, to a lesser extent, Sb compositions, as well as more radiogenic Pb isotopic ratios. Such enrichments are due to contamination by sediment-derived fluids. The sedimentary input is mainly controlled by sediments coming from South America, specifically from the Amazon craton. We propose that this signature is acquired during serpentinization in the first step of subduction ($200 < T < 400$ °C) during mixing between metasediments and serpentinites in the subduction channel.

(3) Mantle wedge serpentinites derive from a highly refractory mantle protolith and serpentine phases were formed essentially from low-Ti olivine and orthopyroxene. The fluids that serpentinized

the mantle wedge present characteristics similar to those of oceanic hydrothermal fluids. We propose that the serpentinization of mantle wedge took place at around 20–25 km, in the stability field of lizardite/chrysotile (T<250–400 °C). At such depth and temperature conditions, the sediments are still releasing their pore fluids (T<200 °C), explaining the relative B-enrichment and the similarity of FME-enrichment with subducted serpentinites, while their structural water incorporated in hydrous mineral (e.g. phengite, lawsonite) remains stable.

Supplementary materials related to this article can be found online at http://dx.doi.org/10.1016/j.chemgeo.2012.04.009.

Acknowledgments

We thank Jean-Luc Devidal (Magmas et Volcans Clermont-Ferrand) for the microprobe analyses and Adeline Besnault (LGCA Grenoble) for the help in the geochemical laboratory. Simone Pourtales and Olivier Bruguier (Géosciences Montpellier) are acknowledged for their help during LA–HR-ICP-MS analyses. We are grateful to Michel Grégoire, Marco Scambelluri and Benoit-Michel Saumur for their constructive scientific discussions. This paper has been greatly improved by L. Reisberg, M. Scambelluri and an anonymous reviewer. The research project was supported by PROCOPE grant and CNRS INSU programs.

References

Abbott Jr., R.N., Draper, G., Broman, B.N., 2006. *P–T* path for ultrahigh-pressure garnet ultramafic rocks of the Cuaba Gneiss, Rio San Juan Complex, Dominican Republic. International Geology Review 48, 778–790.

Agranier, A., Lee, C.-T.A., Li, Z.-X.A., Leeman, W.P., 2007. Fluid mobile element budgets in serpentinized oceanic lithospheric mantle: insights from B, As, Li, Pb, PGEs and Os sotopes in the Feather River Ophiolite, California. Chemical Geology 245, 230–241.

Andreani, M., Godard, M., Mével, C., 2009. LA-(HR-)ICPMS study of serpentinites from ODP Site 920 (23°N MAR): insights on transfers and trace element distribution during serpentinization. Geophysical Research Abstracts EGU 2009 EGU2009-13248.

Arai, S., 1994. Characterization of spinel peridotites by olivine-spinel compositional relationships: review and interpretation. Chemical Geology 113, 191–204.

Arai, S., Ishimaru, S., 2008. Insights into petrological characteristics of the lithosphere of mantle wedge beneath arcs through peridotite xenoliths: a review. Journal of Petrology 49 (4), 665–695.

Auzende, A.-L., Devouard, B., Guillot, S., Daniel, I., Baronnet, A., Lardeaux, J.-M., 2002. Serpentinites from Central Cuba: petrology and HRTEM study. European Journal of Mineralogy 14, 905–914.

Ayuso, R.A., Bevier, M.L., 1991. Regional differences in Pb isotopic compositions of feldspars in plutonic rocks of the Northern Appalachian Mountains, U.S.A., and Canada: a geochemical method of terrane correlation. Tectonics 10 (1), 191–212.

Barnes, J.D., Straub, S.M., 2010. Chlorine stable isotope variations in Izu-Bonin tephra: implications for serpentinites subduction. Chemical Geology 272, 62–74.

Bebout, G.E., Barton, M.D., 1989. Fluid flow and metasomatism in a subduction zone hydrothermal system: Catalina Schist terrane, California. Geology 17, 976–980.

Bebout, G.E., Ryan, J.G., Leeman, W.P., Bebout, A.E., 1999. Fractionation of trace elements by subduction-zone metamorphism—effect of convergent-margin thermal evolution. Earth and Planetary Science Letters 171, 63–81.

Bebout, G.E., Bebout, A.E., Graham, C.M., 2007. Cycling of B, Li, and LILE (K, Cs, Rb, Ba, Sr) into subduction zones: SIMS evidence from micas in high-P/T metasedimentary rocks. Chemical Geology 239, 284–304.

Berman, R.G., Engi, M., Greenwood, H.J., Brown, T.H., 1986. Derivation of internally-consistent thermodynamic data by the technique of mathematical programming: a review with application to the system MgO–SiO_2–H_2O. Journal of Petrology 27, 1331–1364.

Blein, O., Guillot, S., Lapierre, H., Mercier de Lépinay, B., Lardeaux, J.-M., Millan Trujillo, G., Campos, M., Garcia, A., 2003. Geochemistry of the Mabujina Complex, Central Cuba: implications on the Cuban cretaceous arc rocks. Journal of Geology 111, 89–101.

Bodinier, J.-L., Godard, M., 2003. Orogenic, ophiolitic, and abyssal peridotites. In: Carlson, R.W. (Ed.), Treatise on Geochemistry. : Treatise on Geochemistry, vol. 2: Mantle and Core. Elsevier Science Ltd., pp. 103–170.

Bodinier, J.-L., Vasseur, G., Vernières, J., Dupuy, C., Fabriès, J., 1990. Mechanism of mantle metasomatism: geochemical evidence from the Lherz orogenic peridotite. Journal of Petrology 31, 597–628.

Bonatti, E., Lawrence, J.R., Morandi, N., 1984. Serpentinization of oceanic peridotites: temperature dependence of mineralogy and boron content. Earth and Planetary Science Letters 70, 88–94.

Brenan, J.M., Shaw, H.F., Ryerson, F.J., 1995. Experimental evidence for the origin of lead enrichment in convergent-margin magmas. Nature 378, 54–56.

Bromiley, G.D., Pawley, A.R., 2003. The stability in the systems MgO–SiO_2–H_2O (MSH) and MgO–Al_2O_3–SiO_2–H_2O (MASH): the effects of Al^{3+} substitution on high-pressure stability. American Mineralogist 88, 99–108.

Burke, K., 1988. Tectonic evolution of the Caribbean. Annual Review of Earth and Planetary Sciences 16, 201–230.

Cannat, M., Mével, C., Maia, M., Deplus, C., Durand, C., Gente, P., Agrinier, P., Belarouchi, A., Dubuisson, G., Humler, E., Reynolds, J., 1995. Thin crust, ultramafic exposures, and rugged faulting patterns at the the Mid-Atlantic Ridge (22°–24°N). Geology 23, 49–52.

Carlson, R.L., 2001. The abundance of ultramafic rocks in Atlantic Ocean crust. Geophysical Journal International 144, 37–48.

Carpentier, M., Chauvel, C., Mattielli, N., 2008. Pb–Nd isotopic constraints on sedimentary input into the Lesser Antilles arc system. Earth and Planetary Science Letters 272, 199–211.

Chauvel, C., Bureau, S., Poggi, C., 2011. Comprehensive chemical and isotopic analyses of basalt and sediment reference materials. Geostandards and Geoanalytical Research 35, 125–143.

Coleman, R.G., Keith, T.E., 1971. A chemical study of serpentinization—Burro Mountain, California. Journal of Petrology 12 (2), 311–328.

Delacour, A., Früh-Green, G.L., Frank, M., Gutjahr, M., Kelley, D.S., 2008. Sr- and Nd-isotope geochemistry of the Atlantis Massif (30°N, MAR): implications for fluid fluxes and lithospheric heterogeneity. Chemical Geology 254, 19–35.

Deschamps, F., Guillot, S., Godard, M., Chauvel, C., Andreani, M., Hattori, K.H., 2010. In situ characterization of serpentinites from forearc mantle wedges: timing of serpentinization and behavior of fluid-mobile elements in subduction zones. Chemical Geology 269, 262–277.

Deschamps, F., Guillot, S., Godard, M., Andreani, M., Hattori, K.H., 2011. Serpentinites act as sponges for fluid-mobile elements in abyssal and subduction zone environments. Terra Nova 23, 171–178.

Dick, H.J.B., 1989. Abyssal peridotites, very-slow spreading ridges and ocean ridge magmatism. In: Saunders, A.D., Norry, M.J. (Eds.), Magmatism in the Ocean Basins: Geological Society of London Special Publications, 42, pp. 71–105.

Dick, H.J.B., Bullen, T., 1984. Chromian spinel as a petrogenetic indicator in abyssal and alpine type peridotites and spatially associated lavas. Contributions to Mineralogy and Petrology 86, 54–76.

Dick, H.J.B., Natland, J.H., 1996. Late-stage melt evolution and transport in the shallow mantle beneath the East Pacific Rise. In: Mével, C., Gillis, K.M., Meyers, P.S. (Eds.), Proceedings of the Ocean Drilling Program, Scientific Results, 147, pp. 103–134.

Dolan, J.F., Mullins, H.T., Wald, D.J., 1998. Active tectonics of the north-central Caribbean; oblique collision, strain partitioning, and opposing subducted slabs. In: Dolan, J.F., Mann, P. (Eds.), Active Strike–Slip and Collisional Tectonics of the Northern Caribbean: Geological Society of America Special Paper, 326, pp. 1–61.

Draper, G., Nagle, F., 1991. Geology, structure, and tectonic development of the Rio San Juan Complex, northern Dominican Republic. Geological Society of America Special Paper 262, 77–95.

Escartin, J., Cannat, M., 1999. Ultramafic exposures and the gravity signature of the lithosphere near the Fifteen-Twenty Fracture Zone (Mid-Atlantic Ridge, 14°–16.5°N). Earth and Planetary Science Letters 171, 411–424.

Evans, B.W., 1977. Metamorphism of Alpine peridotite and serpentinite. Annual Review of Earth and Planetary Sciences 5, 397–447.

Galer, S.J.G., Abouchami, W., 1998. Practical application of lead triple spiking for correction of instrumental mass discrimination. Mineralogical Magazine 62A, 491–492.

Gammons, C.H., Wood, S.A., Williams, A.E., 1996. The aqueous geochemistry of rare earth elements and yttrium: VI. Stability of neodymium chloride complexes from 25 to 300 degrees C. Geochimica et Cosmochimica Acta 60, 4615–4630.

Garciá-Casco, A., Torres-Roldán, R.L., Iturralde-Vinent, M.A., Millán, G., Nunez Cambra, K., Lázaro, C., Rodriguez Vega, A., 2006. High pressure metamorphism of ophiolites in Cuba. Geologica Acta 4, 63–88.

García-Casco, A., Iturralde-Vinent, M.A., Pindell, J., 2008. Latest Cretaceous collision/accretion between the Caribbean Plate and Caribeana: origin of metamorphic terranes in the Greater Antilles. International Geology Review 50, 781–809.

Garrido, C.J., López Sánchez-Vizcaíno, V., Gómez-Pugnaire, M.T., Trommsdorff, V., Alard, O., Bodinier, J.-L., Godard, M., 2005. Enrichment of HFSE in chlorite–harzburgite produced by high-pressure dehydration of antigorite–serpentinite: implications for subduction magmatism. Geochemistry, Geophysics, Geosystems 6 (1), http://dx.doi.org/10.1029/2004GC000791.

Gillis, K.M., Meyer, P.S., 2001. Metasomatism of oceanic gabbros by late stage melts and hydrothermal fluids: evidence from the rare earth element composition of amphiboles. Geochemistry, Geophysics, Geosystems 2000GC000087.

Godard, M., Lagabrielle, Y., Alard, O., Harvey, J., 2008. Geochemistry of the highly depleted peridotites drilled at ODP Sites 1272 and 1274 (Fifteen-Twenty Fracture Zone, Mid-Atlantic Ridge): implications for mantle dynamics beneath a slow spreading ridge. Earth and Planetary Science Letters 267, 410–425.

Godard, M., Awaji, S., Hansen, H., Hellebrand, E., Brunelli, D., Johnson, K., Yamasaki, T., Maeda, J., Abratis, M., Christie, D., Kato, Y., Mariet, C., Rosner, M., 2009. Geochemistry of a long in-situ section of intrusive slow-spread oceanic lithosphere: results from IODP Site U1309 (Atlantis Massif, 30°N Mid-Atlantic-Ridge). Earth and Planetary Science Letters 279 (110), 122.

Guillot, S., Hattori, K., Agard, P., Schwartz, S., Vidal, O., 2009. Exhumation processes in oceanic and continental subduction contexts: a review. Special Volume, Subduction Zone Geodynamics, Frontiers in Earth Sciences, pp. 175–205.

Hart, S.R., 1984. A large-scale isotopic anomaly in the Southern Hemisphere mantle. Nature 309, 753–757.

Hattori, K.H., Guillot, S., 2003. Volcanic fronts form as a consequence of serpentinite dehydration in the forearc mantle wedge. Geology 31 (6), 525–528.

Hattori, K.H., Guillot, S., 2007. Geochemical character of serpentinites associated with high- to ultrahigh-pressure metamorphic rocks in the Alps, Cuba, and the Himalayas: recycling of elements in subduction zones. Geochemistry, Geophysics, Geosystems 8 (9), http://dx.doi.org/10.1029/2007GC001594.
Hattori, K., Takahashi, Y., Guillot, S., Johanson, B., 2005. Occurrence of arsenic (V) in forearc mantle serpentinites based on X-ray absorption spectroscopy study. Geochimica et Cosmochimica Acta 69 (23), 5585–5596.
Hattori, K.H., Guillot, S., Saumur, B.-M., Tubrett, M.N., Vidal, O., Morfin, S., 2010. Corundum-bearing garnet peridotite from northern Dominican Republic: a metamorphic product of an arc cumulate in the Caribbean subduction zone. Lithos 114, 437–450.
Hellebrand, E., Snow, J.E., Hoppe, P., Hofmann, A., 2002. Garnet-field and late-stage refertilization in 'residual' abyssal peridotites from the Central Indian Ridge. Journal of Petrology 43 (12), 2305–2338.
Ionov, D.A., 2010. Petrology of mantle wedge lithosphere: new data on supra-subduction zone peridotite xenoliths from the andesitic Avacha volcano, Kamchatka. Journal of Petrology 51, 327–361.
Ishii, T., Robinson, P.T., Maekawa, H., Fiske, R., 1992. Petrological studies of peridotites from diapiric serpentinite seamounts in the Izu–Ogasawara–Mariana forearc, Leg 125. In: Fryer, P., Pearce, J.A., Stokking, L.B., et al. (Eds.), Proceedings of the Ocean Drilling Program, Scientific Results, College Station,TX: Ocean Drilling Program, 125, pp. 445–485.
Iturralde-Vinent, M.A., 1994. Circum-caribbean tectonic and igneous activity and the evolution of Caribbean plate: discussion. Geological Society of America Bulletin 85, 1961–1962.
Iturralde-Vinent, M.A., 1998. Sinopsis de la constitución geológica de Cuba. Acta Geologica Hispaniola 33, 9–56.
Iyer, K., Rüpke, L.H., Morgan, J.P., 2010. Feedbacks between mantle hydration and hydrothermal convection at ocean spreading centers. Earth and Planetary Science Letters 296, 34–44.
Jiao, W., Silver, P.G., Fei, Y., Prewitt, C.T., 2000. Do intermediate- and deep-focus earthquakes occur on preexisting weak zones? An examination of the Tonga subduction zone. Journal of Geophysical Research 105, 28,125–28,138.
Jochum, K.P., Stoll, B., 2008. Reference materials for elemental and isotopic analyses by LA-(MC)–ICP-MS: successes and outstanding needs. In: Sylvester, P. (Ed.), Laser Ablation ICP-MS in the Earth Sciences: Current Practices and Outstanding Issues. Mineralogical Association Canada, pp. 147–168.
Jochum, K.P., Verma, S.P., 1996. Extreme enrichment of Sb, Tl and other trace elements in altered MORB. Chemical Geology 130, 289–299.
Jochum, K.P., Willbold, M., Raczek, I., Stoll, B., Herwig, K., 2005. Chemical characterisation of the USGS reference glasses GSA-1G, GSC-1G, GSD-1G, GSE-1G, BCR-2G, BHVO-2G and BIR-1G using EPMA, ID-TIMS, ID–ICPMS and LA–ICPMS. Geostandards and Geoanalytical Research 29 (3), 285–302.
John, T., Scambelluri, M., Frische, M., Barnes, J.D., Bach, W., 2011. Dehydration of subducting serpentinites: implications for halogen mobility in subduction zones and the deep halogen cycle. Earth and Planetary Science Letters, http://dx.doi.org/10.1016/j.epsl.2011.05.038.
Johnson, K.T.M., Dick, H.J.B., Shimizu, N., 1990. Melting in the oceanic upper mantle: an ion microprobe study of diopsides in abyssal peridotites. Journal of Geophysical Research 95 (B3), 2661–2678.
Keppler, H., 1996. Constraints from partitioning experiments on the composition of subduction-zone fluids. Nature 380, 237–240.
Kirby, S.H., Engdahl, E.R., Denlinger, R., 1996. Intermediate-depth intraslab earthquakes and arc volcanism as physical expressions of crustal and uppermost mantle metamorphism in subducting slabs. In: Bebout, G.E., et al. (Ed.), Subduction: Top to Bottom: Geophysical Monograph Series AGU, Washington, D.C., 96, pp. 195–214.
Kodolányi, J., Pettke, T., 2011. Loss of trace elements from serpentinites during fluid-assisted transformation of chrysotile to antigorite—an example from Guatemala. Chemical Geology 284, 351–362.
Kodolányi, J., Pettke, T., Spandler, C., Kamber, B.S., Gméling, K., 2012. Geochemistry of ocean floor and fore-arc serpentinites: constraints on the ultramafic input to subduction zones. Journal of Petrology 53, 235–270.
Kogiso, T., Tatsumi, Y., Nakano, S., 1997. Trace element transport during dehydration processes in the subducted oceanic crust: 1. Experiments and implications for the origin of ocean island basalts. Earth and Planetary Science Letters 148, 193–205.
Komor, S.C., Elthon, D., Casey, J.F., 1985. Serpentinization of cumulate ultramafic rocks from the North Arm Mountain massif of the Bay of Islands ophiolite. Geochimica et Cosmochimica Acta 49, 2331–2338.
Krebs, M., Maresch, W.V., Schertl, H.-P., Münker, C., Baumann, A., Draper, G., Idleman, B., Trapp, E., 2008. The dynamics of intra-oceanic subduction zones: a direct comparison between fossil petrological evidence (Rio San Juan Complex, Dominican Republic) and numerical simulation. Lithos 103, 106–137.
Kretz, R., 1983. Symbols for rock-forming minerals. American Mineralogist 68, 277–279.
Kuhn, et al., 2004. The hydrothermal field-revisited: preliminary results of the R/V Meteor cruise hydromar I (M60/3). Interridge News 13, 1–4.
Leeman, W.P., Sisson, V.B., 1996. In: Grew, E.S., Anovitz, L.M. (Eds.), Boron: Mineralogy, Petrology and Geochemistry. Mineralogical Society of America, Washington, D.C., pp. 645–707.
Leeman, W.P., Carr, M.J., Morris, J.D., 1994. Boron geochemistry of the Central American Volcanic Arc: constraints on the genesis of subduction-related magmas. Geochimica et Cosmochimica Acta 58, 149–168.
Lewis, J.F., Draper, G., Bourdon, C., Bowin, C., Mattson, P.O., Maurrasse, F., Nagle, F., Pardo, G., 1990. Geology and tectonic evolution of the northern Caribbean margin. In: Dengo, G., Case, J.E. (Eds.), The Caribbean Region: Boulder, Colorado, Geological Society of America, The Geology of North America H, pp. 77–140.
Li, Z.-X.A., Lee, C.-T.A., 2006. Geochemical investigation of serpentinized oceanic lithospheric mantle in the Feather River Ophiolite, California: implications for the recycling rate of water by subduction. Chemical Geology 235, 161–185.
Manhès, G., Allègre, C.J., Provost, A., 1984. U–Th–Pb systematics of the eucrite "Juvinas": precise age determination and evidence for exotic lead. Geochimica et Cosmochimica Acta 48, 2247–2264.
Mann, P., 1999. Caribbean sedimentary basins: classification and tectonic setting. In: Mann, P. (Ed.), Caribbean Basins, Sedimentary Basins of the World, 4. Elsevier Science B.V., pp. 3–31.
Mann, P., Draper, G., Lewis, J.F., 1991. An overview of the geologic and tectonic development of Hispaniola. In: Mann, P., Draper, G., Lewis, J.F. (Eds.), Geological and Tectonic Development of the North American–Caribbean Plate Boundary Zone in Hispaniola: Geological Society of America Special Paper, 262, pp. 1–28.
Marchesi, C., Garrido, C.J., Bosch, D., Proenza, J.A., Gervilla, F., Monié, P., Rodriguez-Vega, A., 2007. Geochemistry of cretaceous magmatism in eastern Cuba: recycling of North American continental sediments and implications for subduction polarity in the Greater Antilles paleo-arc. Journal of Petrology 48 (9), 1813–1840.
McDonough, W.F., Sun, S.-S., 1995. The composition of the Earth. Chemical Geology 120, 223–253.
Meschede, M., Frisch, W., 1998. A plate-tectonic model for the Mesozoic and early Cenozoic history of the Caribbean plate. Tectonophysics 296, 269–291.
Mével, C., 2003. Serpentinization of abyssal peridotites at mid-ocean ridges. Comptes Rendus Géoscience 335, 825–852.
Meyerhoff, A.M., Hatten, C.W., 1968. Diapiric structures in Central Cuba. Memoir—American Association of Petroleum Geologists 8, 315–357.
Millan, G., 1993. Evolucion de la estructura del macizo de Escambray, sur de Cuba central. Evolution of the structure of the Escambray Massif, south-central Cuba. Ciencias de la Tierra y del Espacio 21–22, 26–45.
Millán, G., 1997. Geología del macizo metamórfico del Escambray. In: Furrazola Bermúdez, G.F., Núñez Cambra, K.E. (Eds.), Estudios sobre geología de Cuba. Centro Nacional de Información Geológica, La Habana, Cuba, pp. 271–288.
Miyashiro, A., Shido, F., Ewing, M., 1969. Composition and origin of serpentinites from the Mid-Atlantic Ridge near 24 and 30°N. Contributions to Mineralogy and Petrology 23, 117–127.
Morris, A.E.L., Taner, I., Meyerhoff, H.A., Meyerhoff, A.A., 1990. Tectonic evolution of the Caribbean region; Alternative hypothesis. In: Dengo, G., Case, J. (Eds.), The Geology of North America, vol. H, The Caribbean Region, Geological Society of America, pp. 433–457.
Navon, O., Stolper, E., 1987. Geochemical consequences of melt percolation: the upper mantle as a chromatographic column. Journal of Geology 95, 285–307.
Niu, Y., 2004. Bulk-rock major and trace element compositions of abyssal peridotites: implications for mantle melting, melt extraction and post-melting processes beneath Mid-Ocean ridges. Journal of Petrology 45 (12), 2423–2458.
O'Hanley, D.S., 1996. Serpentinites, records of tectonic and petrological history. Oxford Monographs on Geology and Geophysics, 34, p. 277.
Pabst, S., Zack, T., Savov, I.P., Ludwig, T., Rost, D., Vicenzi, E., 2011. Evidence for boron incorporation into the serpentine crystal structure. American Mineralogist 96, 1112–1119.
Paulick, H., Bach, W., Godard, M., Hoog, C.J., Suhr, G., Harvey, J., 2006. Geochemistry of abyssal peridotites (Mid-Atlantic Ridge, 15°20′N, ODP Leg 209): implications for fluid/rock interaction in slow spreading environments. Chemical Geology 234, 179–210.
Peacock, S., 2001. Are the lower planes of double seismic zones caused by serpentine dehydration in subducting oceanic mantle? Geology 29, 299–302.
Pearce, J.A., 1983. Role of the sub-continental lithosphere in magma genesis at active continental margins. In: Hawkesworth, C.J., Norry, M.J. (Eds.), Continental Basalts and Mantle Xenoliths. Shiva, pp. 230–249.
Pelletier, L., Müntener, O., Kalt, A., Vennemann, T.W., Belgya, T., 2008. Emplacement of ultramafic rocks into the continental crust monitored by light and other trace elements: an example from the Geisspfad body (Swiss–Italian Alps). Chemical Geology 255, 143–159.
Pindell, J.L., Barrett, S.F., 1990. Geological evolution of the Caribbean Region; a plate tectonic perspective. In: Dengo, G., Case, J. (Eds.), The Geology of North America, vol. H, The Caribbean Region, Geological Society of America, pp. 405–432.
Pindell, J.L., Draper, G., 1991. Stratigraphy and geological history of the Puerto Plata area, northern Dominican Republic. Geological and Tectonic Development of the North American–Caribbean plate boundary zone in Hispaniola: Geological Society of America Special Paper, 262, pp. 97–114.
Pindell, J.L., Cande, S.C., Pitman III, W.C., Rowley, D.B., Dewey, J.F., LaBrecque, J.L., Haxby, W.F., 1988. A plate-kinematic framework for models of Caribbean evolution. In: Scotese, C.R., Sager, W.W. (Eds.), Tectonophysics, 155, pp. 121–138.
Pindell, J.L., Kennan, L., Maresch, W.V., Stanek, K.P., Draper, G., Higgs, R., 2005. Plate-kinematics and crustal dynamics of circum-Caribbean arc-continent interactions: tectonics controls on basin development in Proto-Caribbean margins. In: Avé Lallemant, H.G., Sisson, V.B. (Eds.), Caribbean-South American Plate Interactions, Venezuela, Boulder, Geological Society of America Special Paper, 394, pp. 7–52.
Piotrowska, K., 1993. Interrelationship of the terranes in western and central Cuba. Tectonophysics 220, 273–282.
Plank, T., Langmuir, C.H., 1998. The chemical composition of subducting sediments and its consequences for the crust and mantle. Chemical Geology 145, 325–394.
Plank, T., Ludden, J.N., 1992. Geochemistry of sediments in the Argo abyssal plain at Site 765: a continental margin reference section for sediment recycling in subduction zones. In: Gradstein, F.M., et al. (Ed.), Proceedings of the Ocean Drilling Program, Scientific results, College Station, Texas, 123, pp. 167–189.
Railsback, L.B., 2003. An earth scientist's periodic table of the elements and their ions. Geology 31 (9), 737–740.

Ranero, C., Morgan, J.P., McIntosh, K., Reichert, C., 2003. Bending-related faulting and mantle serpentinization at the Middle America trench. Nature 425, 367–373.
Ranero, C., Villaseñor, A., Morgan, J.P., Weinrebe, W., 2005. Relationship between bend–faulting at trenches and intermediate-depth seismicity. Geochemistry, Geophysics, Geosystems 6, http://dx.doi.org/10.1029/2005GC000997.
Rehkämper, M., Hofmann, A.W., 1997. Recycled ocean crust and sediment in Indian Ocean MORB. Earth and Planetary Science Letters 147, 93–106.
Ross, M., Scotese, C.R., 1988. A hierarchical tectonic model of the Gulf of Mexico and Caribbean region. Tectonophysics 155, 139–168.
Rüpke, L.H., Morgan, J.P., Hort, M., Connolly, J.A.D., 2004. Serpentine and the subduction zone water cycle. Earth and Planetary Science Letters 223, 17–34.
Salters, V.J.M., Stracke, A., 2004. Composition of the depleted mantle. Geochemistry, Geophysics, Geosystems 5 (5), http://dx.doi.org/10.1029/2003GC000597.
Saumur, B.-M., Hattori, K.H., Guillot, S., 2010. Contrasting origins of serpentinites in a subduction complex, northern Dominican Republic. GSA Bulletin, The Geological Society of America 122, 292–304.
Savage, J.C., 1969. The mechanics of deep-focus faulting. Tectonophysics 8, 115–127.
Savov, I.P., Ryan, J.G., D'Antonio, M., Kelley, K., Mattie, P., 2005. Geochemistry of serpentinized peridotites from the Mariana Forearc Conical Seamount, ODP Leg 125: implications for the elemental recycling at subduction zones. Geochemistry, Geophysics, Geosystems 6 (4), http://dx.doi.org/10.1029/2004GC000777.
Savov, I.P., Ryan, J.G., D'Antonio, M., Fryer, P., 2007. Shallow slab fluid release across and along the Mariana arc-basin system: insights from geochemistry of serpentinized peridotites from the Mariana fore arc. Journal of Geophysical Research 112, http://dx.doi.org/10.1029/2006JB004749.
Sawyer, D.S., Buffler, R.T., Pilger, R.H., 1991. The crust under the Gulf of Mexico basin in Salvador. In: Salvador, A. (Ed.), The Gulf of Mexico basin, the Geology of North America. Geological Society of America, pp. 53–72. vol. J.
Scambelluri, M., Rampone, E., Piccardo, G.B., 2001a. Fluid and element cycling in subducted serpentinite: a trace-element study of the Erro-Tobbio high pressure ultramafites (Western Alps, NW Italy). Journal of Petrology 42 (1), 55–67.
Scambelluri, M., Bottazzi, P., Trommsdorff, V., Vannucci, R., Hermann, J., Gòmez-Pugnaire, M.T., Lòpez-Sànchez Vizcaìno, V., 2001b. Incompatible element-rich fluids released by antigorite breakdown in deeply subducted mantle. Earth and Planetary Science Letters 192, 457–470.
Scambelluri, M., Müntener, O., Ottolini, L., Pettke, T.T., Vannucci, R., 2004a. The fate of B, Cl and Li in the subducted oceanic mantle and in the antigorite breakdown fluids. Earth and Planetary Science Letters 222, 217–234.
Scambelluri, M., Fiebig, J., Malaspina, N., Müntener, O., Pettke, T., 2004b. Serpentinite subduction: implications for fluid processes and trace-element recycling. International Geology Review 46 (7), 595–613.
Schmidt, K., Koschinsky, A., Garbe-Schönberg, D., Carvalho (de), L.M., Seifert, R., 2007. Geochemistry of hydrothermal fluids from the ultramafic-hosted Logatchev hydrothermal field, 15°N on the Mid-Atlantic Ridge: temporal and spatial investigation. Chemical Geology 242, 1–21.
Schneider, J., Bosch, D., Monie, P., Guillot, S., Garcia-Casco, A., Lardeaux, J.-M., Torres-Roldan, R.L., Trujillo, G.M., 2004. Origin and evolution of the Escambray Massif (central Cuba): an example of HP/LT rocks exhumed during intraoceanic subduction. Journal of Metamorphic Geology 22, 227–247.
Somin, M.L., Millán, G., 1981. Geology of the Metamorphic Complexes of Cuba: Moscow, USSR. Nauka Press. 218 pp. (in Russian).
Spear, F.S., 1993. Metamorphic phase equilibria and pressure–temperature–time paths. Mineralogical Society of America, Monograph Series, 799.
Stalder, R., Foley, S.F., Brey, G.P., Horn, I., 1998. Mineral-aqueous fluid partitioning of trace elements at 900–1200 °C and 3.0–5.7 GPa: new experimental data for garnet, clinopyroxene, and rutile, and implications for mantle metasomatism. Geochimica et Cosmochimica Acta 62, 781–801.
Stanek, K.P., Maresch, W.V., Grafe, F., Grevel, C., Baumann, A., 2006. Structure, tectonics and metamorphic development of the Sancti Spiritus Dome (Eastern Escambray massif, Central Cuba). Geologica Acta 4, 151–170.
Stern, R.J., 2002. Subduction zones. Reviews of Geophysics 40 (4), 1012, http://dx.doi.org/10.1029/2001RG000108.
Sun, M., Kerrich, R., 1995. Rare earth element and high field strength element characteristics of whole rocks and mineral separates of ultramafic nodules in Cenozoic volcanic vents of southeastern British Columbia, Canada. Geochimica et Cosmochimica Acta 59 (23), 4863–4879.
Tatsumi, Y., 1986. Migration of fluid phases and genesis of basalt magmas in subduction zones. Journal of Geophysical Research 94 (4), 4697–4707.
Tenthorey, E., Hermann, J., 2004. Composition of fluids during serpentinite breakdown in subduction zones: evidence for limited boron mobility + supplementary data. Geology 32 (10), 865–868.
Tohver, E., Bettencourt, J.S., Tosdal, R., Mezger, K., Leite, W.B., Payolla, B.L., 2004. Terrane transfer during the Greenville orogeny: tracing the Amazonian ancestry of southern Appalachian basement through Pb and Nd isotopes. Earth and Planetary Science Letters 228, 161–176.
Tonarini, S., Agostini, S., Doglioni, C., Innocenti, F., Manetti, P., 2007. Evidence for serpentinite fluid in convergent margin systems: the example of El Salvador (Central America) arc lavas. Geochemistry, Geophysics, Geosystems 8 (9), http://dx.doi.org/10.1029/2006GC001508.
Tonarini, S., Leeman, W.P., Leat, P.T., 2011. Subduction erosion of forearc mantle wedge implicated in the genesis of the South Sandwich Island (SSI) arc: evidence from boron isotope systematics. Earth and Planetary Science Letters 301, 275–284.
Ulmer, P., Trommsdorff, V., 1995. Serpentine stability to mantle depths and subduction-related magmatism. Science 268 (5212), 858–861.
Van Achterberg, E., Ryan, C.G., Jackson, S.E., Griffin, W., 2001. Data reduction software for LA–ICP-MS. In: Sylvester, P. (Ed.), Laser Ablation ICP-MS in the Earth Science. Mineralogical Association of Canada, pp. 239–243.
Van Keken, P.E., Hacker, B.R., Syracuse, E.M., Abers, G.A., 2011. Subduction factory: 4. Depth-dependent flux of H_2O from subducting slabs worldwide. Journal of Geophysical Research 116, http://dx.doi.org/10.1029/2010JB007922.
Vils, F., Pelletier, L., Kalt, A., Müntener, O., Ludwig, T., 2008. The lithium, boron and beryllium content of serpentinized peridotites from ODP Leg 209 (sites 1272A and 1274A): implications for lithium and boron budgets of oceanic lithosphere. Geochimica et Cosmochimica Acta 72, 5475–5504.
Vils, F., Müntener, O., Kalt, A., Ludwig, T., 2011. Implications of the serpentine phase transition on the behaviour of beryllium and lithium–boron of subducted ultramafic rocks. Geochimica et Cosmochimica Acta 75, 1249–1271.
Wunder, B., Schreyer, W., 1997. Antigorite: high-pressure stability in the system MgO–SiO_2–H_2O (MSH). Lithos 41, 213–227.
Wunder, B., Wirth, R., Gottschalk, M., 2001. Antigorite: pressure and temperature dependence of polysomatism and water content. European Journal of Mineralogy 13, 485–495.
Wunder, B., Deschamps, F., Watenphul, A., Guillot, S., Meixner, A., Romer, R.L., Wirth, R., 2010. The effect of chrysotile-nanotubes on the serpentine-fluid Li-isotopic fractionation. Contributions to Mineralogy and Petrology 158, 781–790.